Draft version April 7, 2026
Typeset using LaTeX **twocolumn** style in AASTeX7.0.1

SPURS: Evidence for Clumpy Neutral Envelopes and Ionized IGM Surrounding Little Red Dots in Abell 2744 from Ultra-Deep Rest-UV Spectroscopy

Mengtao Tang [1,2,3] Daniel P. Stark [4] Charlotte A. Mason [5,6] Zuyi Chen [5,6] Harley Katz [7,8] Max Gronke [9] Lukas J. Furtak [10,11] Seok-Jun Chang [12] Jorryt Matthee [13] Lily Whitler [14,15] Adi Zitrin [16] Ryan Endsley [11,10] Viola Gelli [5,6] Tamojeet Roychowdhury [4] Peter Senchyna [17] Michael W. Topping [18] and Meng Zhang [1,2,3]

[1] Tsung-Dao Lee Institute, Shanghai Jiao Tong University, 1 Lisuo Road, Shanghai 201210, People's Republic of China
[2] School of Physics and Astronomy, Shanghai Jiao Tong University, 800 Dongchuan Road, Shanghai 200240, People's Republic of China
[3] State Key Laboratory of Dark Matter Physics, Shanghai Jiao Tong University, 1 Lisuo Road, Shanghai 201210, People's Republic of China
[4] Department of Astronomy, University of California, Berkeley, Berkeley, CA 94720, USA
[5] Cosmic Dawn Center (DAWN)
[6] Niels Bohr Institute, University of Copenhagen, Jagtvej 128, 2200 Copenhagen N, Denmark
[7] Department of Astronomy & Astrophysics, University of Chicago, 5640 S Ellis Avenue, Chicago, IL 60637, USA
[8] Kavli Institute for Cosmological Physics, University of Chicago, Chicago IL 60637, USA
[9] Centre for Astronomy of Heidelberg University, Astronomisches Rechen-Institut, Mönchhofstr. 12-14, 69120 Heidelberg, Germany
[10] Cosmic Frontier Center, The University of Texas at Austin, Austin, TX 78712, USA
[11] Department of Astronomy, The University of Texas at Austin, Austin, TX 78712, USA
[12] Max-Planck-Institut für Astrophysik, Karl-Schwarzschild-Straße 1, D-85748 Garching b. München, Germany
[13] Institute of Science and Technology Austria (ISTA), Am Campus 1, 3400 Klosterneuburg, Austria
[14] Kavli Institute for Cosmology, University of Cambridge, Madingley Road, Cambridge, CB3 0HA, UK
[15] Cavendish Laboratory, University of Cambridge, JJ Thomson Avenue, Cambridge, CB3 0US, UK
[16] Department of Physics, Ben-Gurion University of the Negev, P.O. Box 653, Be'er-Sheva 84105, Israel
[17] The Observatories of the Carnegie Institution for Science, 813 Santa Barbara Street, Pasadena, CA 91101, USA
[18] Steward Observatory, University of Arizona, 933 N Cherry Avenue, Tucson, AZ 85721, USA

ABSTRACT

Rest-frame ultraviolet (UV) spectra of Little Red Dots (LRDs) often show Lyα emission. Along with broad Balmer emission, LRDs are expected to produce broad Lyα emission. However, the large column density of neutral gas invoked to explain the Balmer break should significantly redshift and further broaden the Lyα line, making it challenging to detect without sensitive, moderate-resolution spectra. We present ultra-deep (29 hours) G140M JWST/NIRSpec observations covering the rest-UV of two LRDs in Abell2744 from the SPURS Cycle 4 Large Program. One of our targets is Abell2744-QSO1, a gravitationally-lensed LRD at $z = 7.04$ with faint UV emission ($M_{UV} = -16.9$), and the other source (UNCOVER-2476) is newly-confirmed at $z = 4.02$ with a very bright UV continuum ($M_{UV} = -19.6$). We find that Abell2744-QSO1 has a broad Lyα profile, along with narrow C IV, Fe II λ1786, and O I λ1302 emission. The Lyα profile suggests an origin similar to the broad Hα, but the line is considerably less redshifted than expected from existing dense gas models. We show that the line profile can be explained if the dense neutral gas is clumpy, allowing Lyα to escape by scattering off of the clump surfaces. We find that UNCOVER-2476 has narrow [Ne IV] emission, indicating either a hard radiation field or shocks. We confirm two close neighbors with Lyα emission around Abell2744-QSO1, indicating it traces a dense environment that may have ionized its surrounding IGM. We suggest that LRDs may preferentially trace bubbles carved by their dense environments, contributing to the prevalence of Lyα in the population.

Email: mengtao.tang@sjtu.edu.cn

Keywords: Active galactic nuclei (16) — High-redshift galaxies (734) — Reionization (1383)

1. INTRODUCTION

The launch of JWST (J. P. Gardner et al. 2023; J. Rigby et al. 2023) opened a new window on active galactic nuclei (AGNs) and the growth of supermassive black holes (SMBHs) in the high redshift universe. One of the biggest surprises has been the discovery of the Little Red Dots (LRDs), sources characterized by very red continua in the rest-frame optical, blue colors in the rest-frame ultraviolet (UV), and both broad hydrogen Balmer lines and narrow forbidden lines in the rest-frame optical (e.g., Y. Harikane et al. 2023; J. E. Greene et al. 2024; J. Matthee et al. 2024; D. D. Kocevski et al. 2025; I. Labbe et al. 2025). Application of lower redshift virial relations to the broad line measurements has led to the suggestion that LRDs are associated with galaxies hosting black holes with masses of $\simeq 10^6$ to 10^8 $M_\odot$ (e.g., J. E. Greene et al. 2024; X. Lin et al. 2024; R. Maiolino et al. 2024a; J. Matthee et al. 2024; D. D. Kocevski et al. 2025). Simple estimates of the LRD host properties point to relatively low stellar masses ($\simeq 10^8 - 10^9$ $M_\odot$; e.g., R. Maiolino et al. 2024a; D. D. Kocevski et al. 2025), indicating that the LRDs may trace galaxies with "overmassive" black holes at high redshift. Current measurements of the volume density of LRDs at $z \gtrsim 4$ reveal this may represent a key phase in the early growth of SMBHs (e.g., J. E. Greene et al. 2024; V. Kokorev et al. 2024; H. B. Akins et al. 2025a; D. D. Kocevski et al. 2025; I. Labbe et al. 2025).

However, it has become clear in the last several years that LRD properties differ from those of most lower-redshift AGN. In particular, LRDs are undetected or only weakly detected in X-rays (e.g., T. T. Ananna et al. 2024; M. Yue et al. 2024; H. B. Akins et al. 2025a; R. Maiolino et al. 2025a), lack evidence for hot dust emission in the rest-frame near-infrared (NIR; e.g., P. G. Pérez-González et al. 2024; C. C. Williams et al. 2024; H. B. Akins et al. 2025a), are generally undetected at radio wavelengths (e.g., C. M. Casey et al. 2025; A. J. Gloudemans et al. 2025; D. J. Setton et al. 2025; M. Xiao et al. 2025), and show little variability (e.g., L. J. Furtak et al. 2025; M. Kokubo & Y. Harikane 2025; W. L. Tee et al. 2025; Z. Zhang et al. 2025). They also often do not show evidence for strong high ionization lines (N V, C IV, He II, [Ne IV], [Ne V]) typically seen in AGN (e.g., E. Lambrides et al. 2024; B. Wang et al. 2025a), although there are LRDs which do clearly have hard radiation fields (I. Labbe et al. 2024; H. B. Akins et al. 2025b; M. Tang et al. 2025b; H. Treiber et al. 2025).

One potential explanation for the unique properties of LRDs is related to a large covering fraction of extremely dense gas. The existence of dense absorbing gas surrounding LRDs was first indicated by narrow Hβ and Hα absorption features superimposed on the broad Balmer emission lines (e.g., X. Lin et al. 2024; J. Matthee et al. 2024; X. Ji et al. 2025; D. D. Kocevski et al. 2025; A. J. Taylor et al. 2025; F. D'Eugenio et al. 2026). These can be explained via the presence of neutral gas densities of $\gtrsim 10^9$ cm^{-3} that are capable of collisionally exciting the $n = 2$ atomic level of hydrogen (e.g. I. Juodžbalis et al. 2024; K. Inayoshi & R. Maiolino 2025; X. Ji et al. 2025; R. P. Naidu et al. 2025). If such dense gas is present, there should also be strong continuum absorption at the Balmer limit. As the first prism spectra of LRDs emerged, it became clear that many indeed exhibit strong Balmer breaks (e.g., L. J. Furtak et al. 2024; I. Juodžbalis et al. 2024; I. Labbe et al. 2024; B. Wang et al. 2024; A. de Graaff et al. 2025a; R. P. Naidu et al. 2025), confirming the impact that dense gas has in shaping the LRD spectrum.

If the AGN is fully enshrouded and column densities are large enough to thermalize the radiation, a quasi-blackbody spectrum may be formed, with effective temperature of $T_{\rm eff} \simeq 5000$ K that is set by hydrogen opacity (e.g., A. de Graaff et al. 2025b; K. Inayoshi et al. 2026; D. Kido et al. 2025; H. Liu et al. 2025; H. Umeda et al. 2026a). In this case, the red optical continuum of LRDs corresponds to the Wien tail of the spectrum, and the absence of X-rays and hot dust emission naturally follows from the Compton thick column densities. It has been argued that the Balmer lines may be broadened via electron scattering as they traverse ionized regions within the column of dense gas (e.g., S.-J. Chang et al. 2026; V. Rusakov et al. 2026; A. Sneppen et al. 2026; A. Torralba et al. 2026a). In this case, the intrinsic line widths may be significantly narrower than measured, and potentially decoupled from the mass, which in turn may suggest that many LRDs may have lower black hole masses than inferred via the virial relations (e.g., F. D'Eugenio et al. 2025a; V. Kokorev et al. 2025; R. P. Naidu et al. 2025; V. Rusakov et al. 2026; c.f., M. Brazzini et al. 2025).

While the dense-gas cocoon model provides a plausible framework for many properties of LRDs, the picture is still not universally accepted and key questions remain, with several non-AGN scenarios also proposed (e.g., L. Zwick et al. 2025; J. Chisholm et al. 2026; D. Nandal & A. Loeb 2026). New constraints on the dense gas coverage are required to stress-test the emerging picture. Lyα is well known to provide a sensitive probe of dense neutral gas (e.g., D. A. Neufeld 1990; M. Dijkstra 2017). If the neutral hydrogen column densities are as large as required to explain the Balmer break and line absorption ($\gtrsim 10^{24}$ cm^{-2}; e.g., I. Juodžbalis et al. 2024; K. Inayoshi & R. Maiolino 2025; X. Ji et al. 2025), the Lyα line will undergo substantial resonant scattering as it traverses the dense gas, significantly altering the line profile with respect to the broad Balmer lines (T. F. Adams 1972; D. A. Neufeld 1990; A. Verhamme et al. 2006). While Lyα has been detected in many LRDs (e.g., V. Kokorev et al. 2023; L. J. Furtak et al. 2024; Y. Asada et al. 2026), very few have been observed at the spectral resolution and depth required to test the predictions of the dense gas cocoon picture (T. Morishita et al. 2026; A. Torralba et al. 2026b).

The high ionization lines provide another probe of the dense gas cocoon picture. If the LRD continuum is associated with a photosphere with $T_{\rm eff} \simeq 5000$ K, we should not expect hard radiation to be transmitted to the narrow-line emitting region. However, as noted above, several very high ionization emission lines have been detected in LRD prism and shallow grating spectra (I. Labbe et al. 2024; H. B. Akins et al. 2025b; E. Lambrides et al. 2025; M. Tang et al. 2025b; H. Treiber et al. 2025). The origin of these high ionization lines is not known. Stellar populations can produce hard photons capable of powering strong C IV and He II, but emission lines that probe above the He$^+$-ionizing edge (> 54 eV) are more likely to be linked to accretion onto a supermassive black hole (e.g., A. Feltre et al. 2016). The presence of very high ionization lines may point to a non-uniform coverage of dense neutral gas, suggesting that at least some LRDs may not be fully enshrouded in gas cocoons. Unfortunately little is known about how commonly LRDs exhibit emission from the most prominent high ionization lines (i.e., N V, C IV, He II, [Ne IV], [Ne V]) given the limited sensitivity of the low resolution prism (see M. Tang et al. 2025b for discussion). In cases where permitted high ionization (i.e., C IV, He II) lines have been detected in prism spectra, the resolution has obscured whether the lines originate in the broad line region (BLR), or whether they reflect the escape of hard photons to the narrow line region (NLR).

Progress requires deep observations of LRDs in the rest-frame UV using higher spectral resolution than has been obtained to-date. In this paper, we present the first results from our Cycle 4 program the SPectroscopic Ultra-deep Reionization-era Survey (SPURS; GO 9214, PIs: C. Mason, D. Stark). SPURS provides ultra deep (29 hours) median-resolution ($R \simeq 1000$) grating spectra in G140M. One of our goals is to obtain robust constraints on the Lyα and very high ionization UV emission lines (N V, C IV, He II, [Ne IV], [Ne V]) in the rest-frame UV spectra of LRDs and broad-line AGNs at high redshift. Here we focus on the observations of two LRDs behind the lensing galaxy cluster Abell 2744: Abell2744-QSO1 and UNCOVER-2476. Abell2744-QSO1 was first identified as an extremely red and compact object in L. J. Furtak et al. (2023a) from the Ultra-deep NIRSpec and NIRCam ObserVations before the Epoch of Reionization (UNCOVER) survey (GO 2561, PIs: I. Labbé, R. Bezanson; R. Bezanson et al. 2024). Subsequent NIRSpec (P. Jakobsen et al. 2022; T. Böker et al. 2023) low-resolution ($R \sim 100$) prism spectroscopy revealed a strong Lyα emission, broad Hβ and Hα emission, and strong Balmer break feature at $z = 7.04$ (L. J. Furtak et al. 2024). High-resolution ($R \simeq 2700$) G395H integral field unit (IFU) spectroscopy further revealed Hβ and Hα absorption lines in Abell2744-QSO1 (F. D'Eugenio et al. 2025a; X. Ji et al. 2025). UNCOVER-2476 was photometrically identified in I. Labbe et al. (2025) at $z_{\rm phot} = 4.56$. Rest-frame UV grating spectroscopy has not been obtained for either of these two LRDs, and UNCOVER-2476 has yet to be observed with any spectrograph.

The organization of this paper is as follows. In Section 2, we describe SPURS observations of Abell2744-QSO1 and UNCOVER-2476, the basic physical properties of these two LRDs, as well as two newly identified galaxies nearby Abell2744-QSO1. We then characterize the rest-frame UV spectroscopic properties of Abell2744-QSO1 and UNCOVER-2476 from SPURS in Section 3. We investigate the H I gas properties inferred from the Lyα emission of Abell2744-QSO1 in Section 4, and discuss the implications for the environment and structure of LRDs in Section 5. Finally, we summarize our conclusions in Section 6. Throughout the paper we adopt a Λ-dominated, flat universe with $\Omega_\Lambda = 0.7$, $\Omega_{\rm M} = 0.3$, and $H_0 = 70$ km s^{-1} Mpc^{-1}. All magnitudes are quoted in the AB system (J. B. Oke & J. E. Gunn 1983) and all equivalent widths (EWs) are quoted in the rest frame.

2. OBSERVATIONS AND DATA ANALYSIS

2.1. *Spectroscopic Observations*

We describe the JWST/NIRSpec spectroscopic data of Abell2744-QSO1 (RA = 3.583540, Dec = −30.396677)[19] and UNCOVER-2476 (RA = 3.610205,

[19] Abell2744-QSO1 is triply imaged by the galaxy cluster Abell 2744, and we target the mostly strongly lensed image ("image B" in L. J. Furtak et al. 2023a) in SPURS observations.

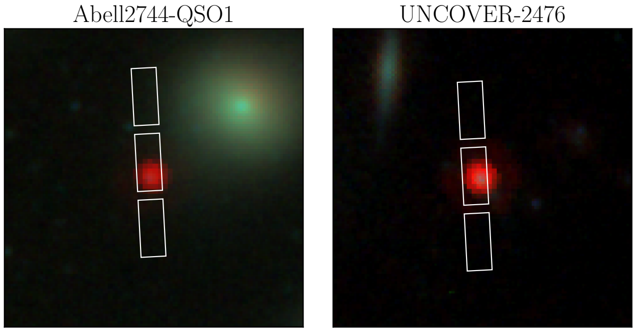

Figure 1. JWST/NIRCam RGB (F444W/F200W/F115W) images ($2.4'' \times 2.4''$) of Abell2744-QSO1 (left) and UNCOVER-2476 (right). We overplot our NIRSpec shutters (white) in SPURS observations. Abell2744-QSO1 is triply imaged by Abell 2744 and we target its the mostly strongly magnified image ('image B" in L. J. Furtak et al. 2023a).

Dec = −30.421001) that were obtained as part of SPURS program (Figure 1). The spectra were obtained using NIRSpec in multi-object spectroscopy mode in 2025 November. We observed one microshutter assembly (MSA; P. Ferruit et al. 2022) mask configuration in the Abell 2744 field, with Abell2744-QSO1 as one of the primary targets. We briefly summarize the SPURS NIRSpec observations of the two LRDs below. A full description of the SPURS program will be presented in a future paper.

The NIRSpec observations were conducted using the medium-resolution ($R \simeq 1000$, corresponding to $\simeq 300$ km s^{-1} per resolution element) grating/filter pairs G140M/F100LP, G235M/F170LP, and G395M/F290LP. We used the three-shutter nod pattern for dithering, which is appropriate for compact high redshift targets. The total on-target integration time is 29.2 hours, 7.9 hours, and 2.9 hours for G140M, G235M, and G395M, respectively.

We reduced the 2D G140M and G235M + G395M spectra separately. We first reduced the G140M spectra following the approaches described in M. W. Topping et al. (2025) which are based on the standard JWST data reduction pipeline[20] (H. Bushouse et al. 2024). This is customized to produce a pixel size of 3.5 Å in the spectral direction for G140M, which is optimal for characterizing the line profiles of Lyα and UV emission for the two LRDs. The G235M and G395M spectra were reduced following the procedures and setup described in A. de Graaff et al. (2025c); K. E. Heintz et al. (2025) using the latest version of `msaexp`[21] package (G. Brammer 2023), which is also based on the standard pipeline. Our reduction with `msaexp` results in a slightly coarser dispersion (6 Å in G140M), but its extended wavelength extraction allows us to achieve longer wavelengths than the normal coverage of each grating. The reduced G235M and G395M spectra cover $1.63-3.02$ μm and $2.80-5.46$ μm, respectively. This allows us to cover the Hα emission of Abell2744-QSO1 (5.28 μm) which will be discussed in the following sections. We confirm that the emission line fluxes and widths measured from the spectra reduced by these two methods are identical. We assumed a point source pathloss correction, motivated by the compact morphology of LRDs (Figure 1).

The 1D spectra of the two LRDs were extracted from the reduced 2D spectra using a boxcar extraction with an aperture of 5 pixels, corresponding to $\sim 0.5''$ in the spatial direction. For G140M spectra, the median 3σ limiting flux for an unresolved emission line (in spectral direction) of a point source is 1.0×10^{-19} erg s^{-1} cm^{-2}. This allows us to detect very weak emission lines in the rest-frame UV for Abell2744-QSO1 (EW = 2.9 Å) and UNCOVER-2476 (EW = 0.9 Å). The median 3σ limiting flux of G235M spectra is 1.9×10^{-19} erg s^{-1} cm^{-2}, corresponding to a limiting EW of 9.9 Å for Abell2744-QSO1 and 2.6 Å for UNCOVER-2476. While most of our focus will be on the two bluer gratings, we also note that the G395M spectra reach a median 3σ limiting flux of 2.0×10^{-19} erg s^{-1} cm^{-2}.

The two LRD spectra have numerous emission lines, which we characterize as follows. For a line detected with S/N > 5, we measure the line flux, centroid, width, and EW by fitting the line profile and nearby continuum with a Gaussian function. In case of emission lines that are close in wavelength or an emission line that shows a complex profile, we fit the line profile with multiple Gaussians simultaneously. If an emission line is detected with lower S/N (< 5), we compute the line fluxes using direct integration. Recent studies have found that the broad Balmer lines of LRDs are better fitted by exponential wings or double-Gaussian profiles when the S/N is high enough (e.g., F. D'Eugenio et al. 2025a,b; V. Kokorev et al. 2025; J. Matthee et al. 2026; V. Rusakov et al. 2026). For the SPURS spectra of the two LRDs, we note that the line fluxes, EWs, and widths inferred from Gaussian fitting are similar to that inferred from exponential fitting. Therefore, we choose to use results from Gaussian fitting in this work, leaving a more detailed analysis of the broad Balmer line profiles to a future paper. Finally, the uncertainties of line fluxes and EWs are evaluated as follows. We resample the flux densities of each spectrum 1000 times by taking the observed value as the mean and the error as the standard devi-

[20] https://github.com/spacetelescope/jwst
[21] https://github.com/gbrammer/msaexp

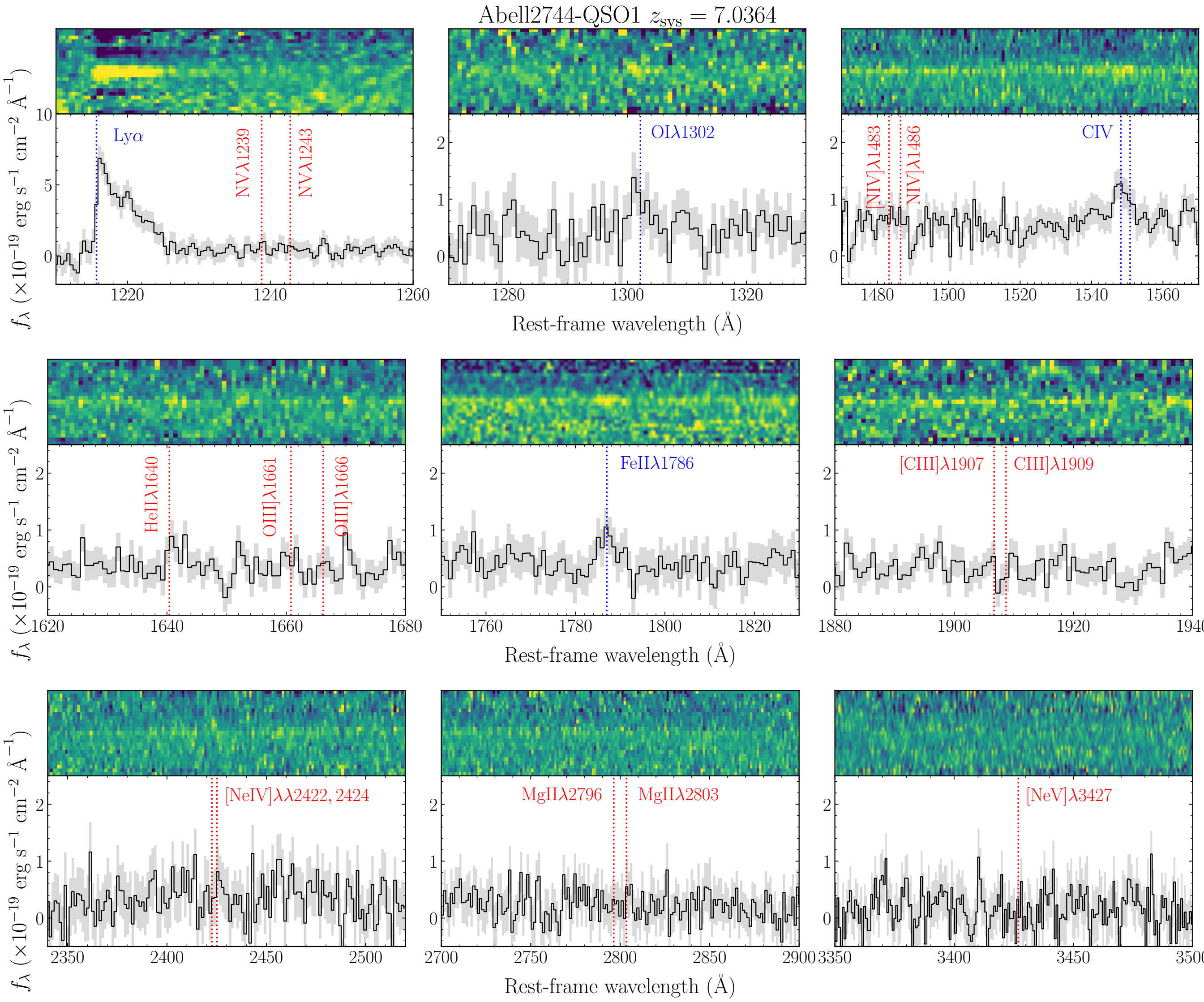

Figure 2. Deep JWST/NIRSpec rest-frame UV (G140M/F100LP and part of G235M/F170LP) spectra of Abell2744-QSO1 obtained from SPURS program. In each panel, we show the 2D spectrum at the top and the 1D at the bottom. The rest-frame UV continuum is marginally detected. We detect the Lyα, O I λ1302, C IV $\lambda\lambda$1548, 1551, and Fe II λ1786 emission lines, overplotting their expected positions from the systemic redshift ($z_{\rm sys}$ = 7.0364) with blue dotted lines. We also plot the expected positions of non-detections (N V, N IV], He II, O III], C III], [Ne IV], Mg II, [Ne V]) with red dotted lines.

ation. Then we compute the line fluxes and EWs from the resampled spectra of each source using the same approach described above. We take the standard deviation of these measurements as the uncertainty. The line fluxes and uncertainties reported throughout the paper are not corrected for gravitational magnification.

2.2. *Physical Properties of LRDs in SPURS*

We briefly describe the basic physical properties of Abell2744-QSO1 and UNCOVER-2476, before discussing their deep rest-frame UV (G140M and part of G235M) spectra (Figure 2 and 3) in the following sections. Since the primary goal of this paper is the rest-frame UV, we defer a complete analysis of the SPURS rest-frame optical (G395M and part of G235M) spectra to a future paper. In the case of UNCOVER-2476, we describe more results from the rest-frame optical spectrum since this source had not been confirmed spectroscopically previously. In contrast, Abell2744-QSO1 has been studied with deep rest-frame optical spectroscopy (F. D'Eugenio et al. 2025a; X. Ji et al. 2025; I. Juodžbalis et al. 2025; R. Maiolino et al. 2025b), so here we primarily review basic properties from the literature, noting consistency with our new rest-frame optical spectrum.

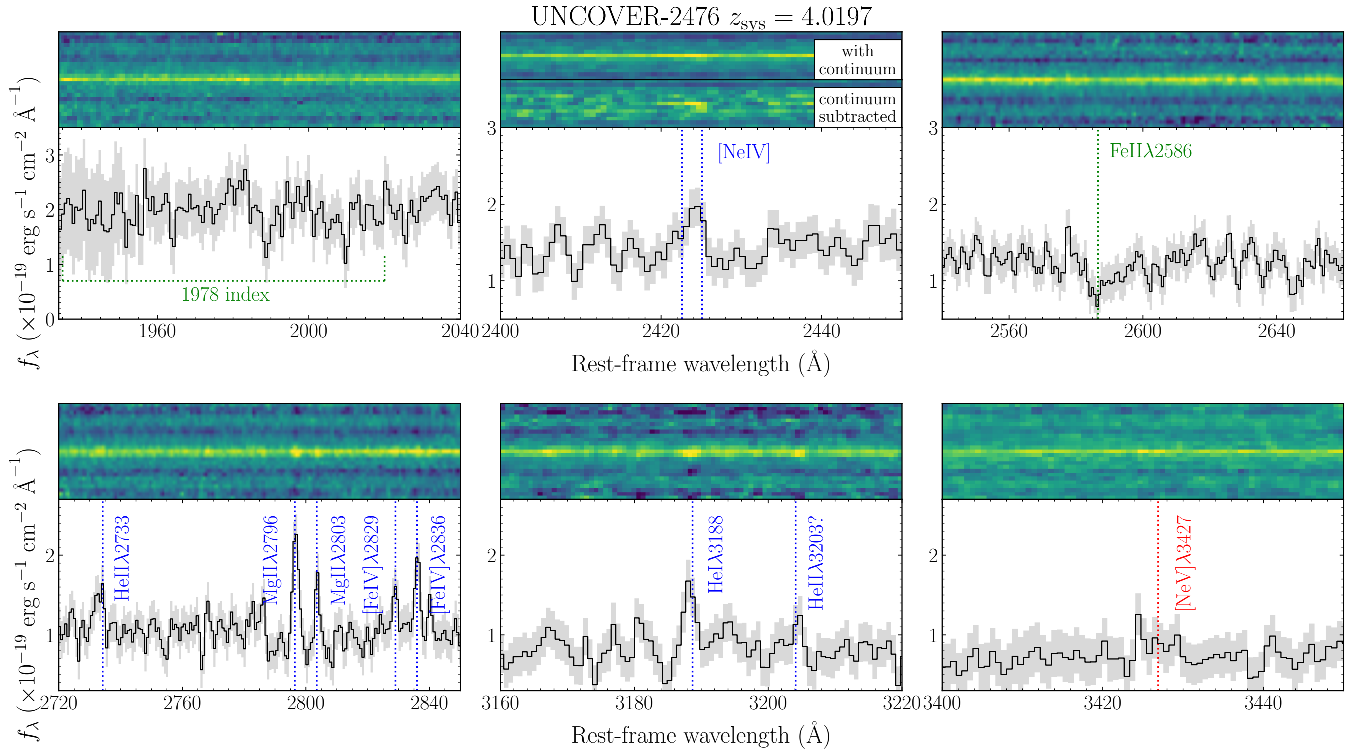

Figure 3. Deep JWST/NIRSpec rest-frame UV (G140M/F100LP) spectrum of UNCOVER-2476 obtained from SPURS program, shown in the same way as Figure 2. The rest-frame UV continuum is clearly detected. We also detect [Ne IV] $\lambda2422, 2424$, He II $\lambda2733$, Mg II $\lambda2796, 2803$, [Fe IV] $\lambda2829, 2836$, He I $\lambda3188$ emission lines (blue), and tentatively detect He II $\lambda3203$. For [Ne IV] (top middle panel), we present both the original 2D spectrum with continuum trace and the continuum-subtracted 2D spectrum, the later of which show the [Ne IV] emission more clearly. [Ne V] $\lambda3427$ is not detected (red dotted line). We mark the 1978 index photospheric absorption and the Fe II $\lambda2586$ absorption line with the green dashed lines.

2.2.1. *Abell2744-QSO1*

Abell2744-QSO1 is extremely faint in rest-frame UV continuum ($M_{\rm UV} = -16.9$; L. J. Furtak et al. 2023a), with the lowest UV luminosity among the LRD population at high redshift (Figure 4). The image we targeted is highly magnified, with a magnification factor of $\mu = 7.2$ derived using the L. J. Furtak et al. (2023b) lens models, which are updated with UNCOVER spectroscopic redshifts in S. H. Price et al. (2025). R100 prism and R2700 G395H IFU observations show broad Hβ and Hα emission (full width at half maximum FWHM $\simeq$ 2700 km s^{-1}) with narrow [O III] $\lambda5007$ line (L. J. Furtak et al. 2024; F. D'Eugenio et al. 2025a; X. Ji et al. 2025). The [O III] $\lambda5007$ is very weak relative to the narrow Hβ emission, likely indicating a very low metallicity for the narrow line emitting gas. R. Maiolino et al. (2025b) estimate the metallicity may be as low as $\simeq 4 \times 10^{-3}\ Z_\odot$ based on the calibrations for [O III]/Hβ (I. H. Laseter et al. 2024; R. L. Sanders et al. 2024). The prism spectrum also revealed a strong Balmer break feature, with a strength ($f_{\nu,4050}/f_{\nu,3640} > 2.3$; L. J. Furtak et al. 2024; F. D'Eugenio et al. 2025a) that is among the upper 15% of the values observed in LRDs (Figure 4; A. de Graaff et al. 2025b). The G395H IFU spectrum further revealed strong absorption lines in both Hβ (EW $= -5.5$ Å; X. Ji et al. 2025) and Hα (EW $= -30$ Å; F. D'Eugenio et al. 2025a). Recent studies have suggested that the strong Balmer break and Balmer line absorption can be described by AGN emission absorbed by very dense gas (e.g., K. Inayoshi & R. Maiolino 2025; X. Ji et al. 2025; R. P. Naidu et al. 2025). We will test this picture with our deep R1000 spectroscopy at rest-frame UV in the following sections.

The SPURS G395M spectrum (covering rest-frame $3500 - 6800$ Å) of Abell2744-QSO1 confirms the presence of broad Hβ and Hα emission with a weak, narrow [O III] $\lambda5007$ line (Figure B2), consistent with earlier prism and G395H IFU observations. We derive a systemic redshift of $z_{\rm sys} = 7.0364$ from the narrow forbidden [O III] $\lambda5007$ line in the G395M spectrum, in good agreement with G395H IFU measurement ($z = 7.0367$; F. D'Eugenio et al. 2025a). We will adopt this systemic redshift for Abell2744-QSO1 throughout the paper. We also confirm that the broad Hα line width in our G395M spectrum (FWHM$_{\rm H\alpha,broad} = 2653 \pm 345$ km s^{-1}) is consistent with G395H IFU measurements. In Section 3.1,

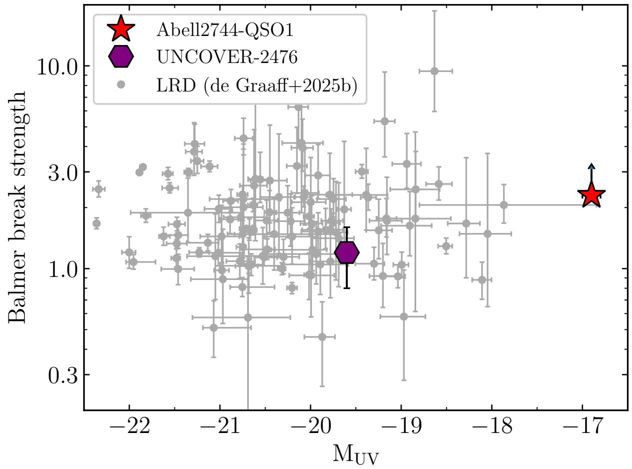

Figure 4. $M_{\rm UV}$ versus Balmer break strength (defined by $f_{\nu,4050}/f_{\nu,3640}$ ratio) of the full LRD population. Abell2744-QSO1 is shown as the red star, with extremely faint rest-frame UV continuum and large Balmer break strength. UNCOVER-2476 is shown as the purple hexagon, with bright UV continuum and relatively small Balmer break strength. We overplot the $z \sim 2-9$ LRD data from A. de Graaff et al. (2025b) as grey circles.

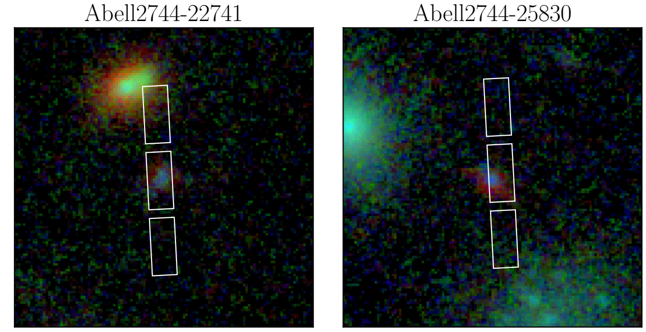

Figure 5. JWST/NIRCam RGB (F444W/F200W/F115W) images ($2.4'' \times 2.4''$) of the two new $z \simeq 7.04$ galaxies identified from SPURS: Abell2744-22741 (left) and Abell2744-25830 (right). We overplot our NIRSpec shutters (white) in SPURS observations.

we will compare the rest-frame UV line profiles to the broad Hα. We report the rest-frame optical emission line fluxes, EWs, and widths measured from our G395M spectrum of Abell2744-QSO1 in Table B2.

2.2.2. *UNCOVER-2476*

The SPURS observations have obtained the first spectrum of UNCOVER-2476. The G235M and G395M spectra (covering rest-frame $3250-10950$ Å) reveal a suite of rest-frame optical to NIR emission lines including broad Hβ and Hα emission with narrow forbidden lines (Figure A1), as is often seen in broad line AGN and LRDs. Using the strong narrow [O III] doublet, we derive a systemic redshift of $z_{\rm sys} = 4.0197$. We measure a FWHM of 1703 ± 28 km s^{-1} (2123 ± 496 km s^{-1}) for the broad Hα (Hβ) line, similar to the typical broad line width seen in LRDs (FWHM $\simeq 2000$ km s^{-1}; e.g., J. E. Greene et al. 2024; X. Lin et al. 2024; R. Maiolino et al. 2024a; J. Matthee et al. 2024; R. E. Hviding et al. 2025; D. D. Kocevski et al. 2025). We report the rest-frame optical to NIR emission line measurements of UNCOVER-2476 in Table A1. In the following, we aim to briefly characterize the rest-frame optical spectroscopic properties of UNCOVER-2476. We leave a more detailed description of the rest-frame optical spectrum in Appendix A.

UNCOVER-2476 is much brighter in rest-frame UV continuum ($M_{\rm UV} = -19.6$) relative to Abell2744-QSO1, comparable to the typical $M_{\rm UV}$ ($\simeq -20$) of the LRD population (Figure 4; A. de Graaff et al. 2025b). Its image is moderately magnified, with a magnification factor of $\mu = 1.9$. The G235M spectrum reveals strong narrow emission lines in rest-frame optical. We measure a large [O III] λ5007 EW of 673 ± 5 Å. This is not only much larger than the EW of Abell2744-QSO1 (5.0 ± 1.5 Å), but also among the upper 10% of the EWs observed in LRDs (A. de Graaff et al. 2025b). We also detect a strong (EW $= -6.6 \pm 0.9$ Å), narrow (FWHM $= 184 \pm 92$ km s^{-1}) Hα absorption line that is blueshifted (-257 ± 92 km s^{-1}) from the line center (Appendix A). Recent studies have pointed to a connection between Balmer absorption feature and Balmer break in LRDs, suggesting the absorption by dense gas as a potential explanation (e.g., A. de Graaff et al. 2025a; K. Inayoshi & R. Maiolino 2025; X. Ji et al. 2025; R. P. Naidu et al. 2025). However, we do not detect a strong Balmer break feature for UNCOVER-2476. From our G235M spectrum, we measure a Balmer break strength that is close to unity ($f_{\nu,4050}/f_{\nu,3640} = 1.2 \pm 0.4$; Figure 4). This is much weaker than the Balmer breaks of many well-studied LRDs with Balmer absorption lines ($f_{\nu,4050}/f_{\nu,3640} \simeq 3-10$; L. J. Furtak et al. 2024; I. Labbe et al. 2024; B. Wang et al. 2024, 2025b; A. de Graaff et al. 2025a; R. P. Naidu et al. 2025). We will further characterize the properties of UNCOVER-2476 with deep rest-frame UV spectrum in Section 3.2.

2.3. *Two New $z \simeq 7.04$ Galaxies Near Abell2744-QSO1*

From SPURS observations on the Abell 2744 field, we also newly identify two galaxies at redshifts that are close to Abell2744-QSO1 ($z \simeq 7.04$): Abell2744-22741 (RA $= 3.625925$, Dec $= -30.393111$) and Abell2744-25830 (RA $= 3.598496$, Dec $= -30.412591$). We present these in this paper, owing to implications for the Lyα visibility of Abell2744-QSO1. The photometry of these

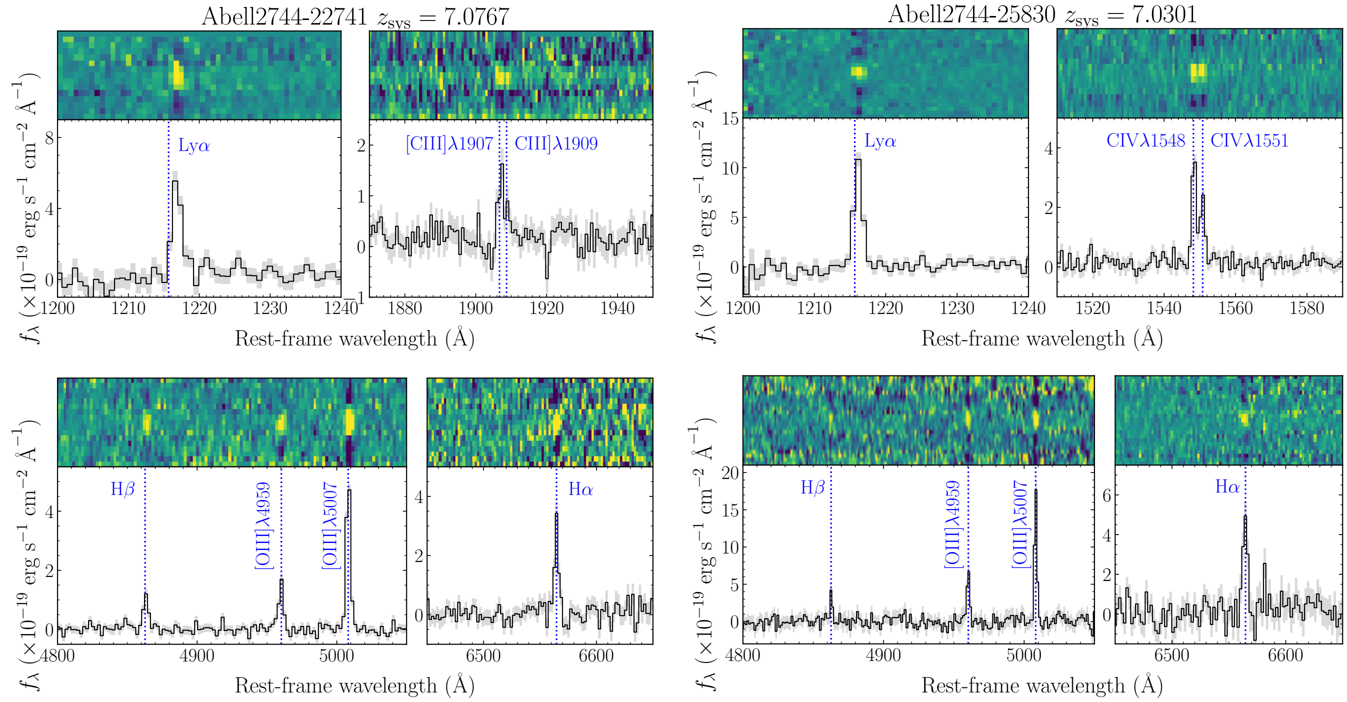

Figure 6. SPURS spectra of the two galaxies nearby Abell2744-QSO1: Abell2744-22741 (left four panels) and Abell2744-25830 (right four panels). For each object, we show the rest-frame UV (G140M) spectrum at the top and the rest-frame optical (G395M) at the bottom. Lyα and strong rest-frame optical emission lines (Hβ, [O III], Hα) are detected in both systems. We additionally detect C III] in Abell2744-22741 and C IV in Abell2744-25830. Spectra are shown in the same way as Figure 2.

two sources was initially characterized in R. Endsley et al. (2025), identifying them as $z \sim 7$ candidates. The SPURS observations have obtained the first spectra of these two sources (Figure 5). We briefly describe the spectroscopic properties of these two systems in this subsection, with the goal of understanding the galaxy environment associated with Abell2744-QSO1.

Abell2744-22741 is more UV-luminous ($M_{UV} = -18.8$) than Abell2744-QSO1. We present the SPURS spectra of Abell2744-22741 in the left panels of Figure 6. This galaxy is 0.68 physical Mpc (pMpc) away from Abell2744-QSO1 in the source plane after correcting for gravitational deflection with the updated L. J. Furtak et al. (2023b) lens models. The G395M (rest-frame optical) spectrum reveals a suite of emission lines (e.g., Hβ, [O III] λ4959, [O III] λ5007, Hα), identifying that this galaxy is at $z_{sys} = 7.0767$. The rest-frame optical emission lines are strong, with an [O III]+Hβ EW (843 ± 42 Å) that is larger than the median EW of $z \sim 7$ galaxies with similar UV luminosities ($\simeq 500 - 600$ Å at $M_{UV} \simeq -18.6$; R. Endsley et al. 2024; R. Begley et al. 2025). This likely suggests that Abell2744-22741 is dominated by very young stellar populations or an AGN which is able to produce an intense radiation field. We see additional evidence of intense radiation field from the rest-frame UV (G140M) spectrum. We detect the [C III], C III] doublet emission. The total C III] EW is 25 ± 4 Å, greater than the majority of $z \sim 7$ galaxies (median C III] EW $\simeq 8$ Å; G. Roberts-Borsani et al. 2024; M. Tang et al. 2025a). We also identify Lyα emission line (EW $= 17 \pm 2$ Å) in the G140M spectrum. The Lyα peak flux is offset by $+227 \pm 92$ km s^{-1} from the line center, comparable to the typical Lyα velocity offset of $z > 6$ galaxies (e.g., A. Saxena et al. 2024; M. Tang et al. 2024a). If the intense radiation field of Abell2744-22741 is able to enhance the ionization fraction of the surrounding IGM, it may boost the Lyα transmission of this system and even that of Abell2744-QSO1.

Abell2744-25830 is much fainter, with a UV luminosity ($M_{UV} = -17.0$) comparable to that of Abell2744-QSO1. This galaxy is even closer to Abell2744-QSO1, which is only 0.16 pMpc away in the source plane. Using the rest-frame optical emission line detections (Hβ, [O III] λ4959, [O III] λ5007, Hα) of Abell2744-25830 (right panels of Figure 6), we derive a systemic redshift of $z_{sys} = 7.0301$. The rest-frame optical emission lines of this system are extremely strong. We derive a very large [O III]+Hβ EW (3518 ± 217 Å), with a value among the upper 1% of EWs observed at $z \sim 7$ (R. Endsley et al. 2024). Such strong [O III]+Hβ emission is often linked to strong C IV emission in cases where the metallicity is low (M. W. Topping et al. 2025). In the rest-frame UV spectrum of Abell2744-25830, we detect a C IV doublet with an extremely large EW (68 ± 6 Å). This indicates a very hard radiation field, which may potentially create a large reionized bubble. We identify a strong Lyα emission for Abell2744-25830. Its Lyα peak flux is only offset by $+123\pm92$ km s^{-1} from the line center, smaller than the majority of the Lyα emitters at $z>7$. The Lyα EW (166 ± 9 Å) is atypically large among the $z\sim7$ population (e.g., L. Napolitano et al. 2024; M. Tang et al. 2024b; G. C. Jones et al. 2025), as expected if the Lyα production is boosted by the hard radiation field and/or the transmission is enhanced in large ionized bubble.

To summarize, both the two newly identified $z\simeq7.04$ galaxies nearby Abell2744-QSO1 appear to have intense radiation fields, especially Abell2744-25830 which is closer to Abell2744-QSO1. These two systems may be part of an overdensity of galaxies that is contributing to the reionization of the IGM surrounding Abell2744-QSO1, aiding the Lyα to escape when the Universe was partially neutral. We will describe the SPURS Lyα measurement of Abell2744-QSO1 in Section 3.1 and discuss the Lyα profile in Section 4.

3. DEEP REST-FRAME UV SPECTRA OF LRDS

3.1. *Abell2744-QSO1*

We now discuss the features in the SPURS rest-frame UV spectrum of Abell2744-QSO1 (Figure 2). We consider both the G140M and part of the G235M data, probing rest-frame wavelengths of $1200-2050$ Å and $2030-3500$ Å, respectively. We visually search the spectrum for emission lines using the systemic redshift ($z_{\rm sys}=7.0364$, Section 2.2.1). An extremely broad Lyα emission line profile is detected with its flux peaking at an observed wavelength of 9778 Å (S/N = 23). We identify iron emission multiplets, Fe II near rest-frame 1786 Å (S/N = 4). We detect the C IV emission line (S/N = 4), although we do not cleanly resolve the doublet. We additionally report an emission line at observed wavelength of 10460 Å (S/N = 3), close to the expected position of O I λ1302. We report the rest-frame UV emission line flux, EW, and FWHM measurements in Table 1.

Table 1. Rest-frame UV emission line flux ($\times10^{-20}$ erg s^{-1} cm^{-2}), EW (Å), and FWHM (km s^{-1}) of Abell2744-QSO1 measured from SPURS spectra.

Line	Flux	EW	FWHM
narrow Lyα	85.2 ± 8.1	23.8 ± 2.3	333 ± 48
broad Lyα	319.0 ± 15.6	88.9 ± 4.3	1498 ± 145
N V λ1239	<15.5	<4.3	-
N V λ1243	<15.7	<4.4	-
O I λ1302	17.6 ± 5.4	3.6 ± 1.1	348 ± 95
[N IV] λ1483	<13.9	<3.2	-
N IV] λ1486	<13.2	<3.0	-
C IV λ1549[b]	25.4 ± 6.0	5.7 ± 1.3	-
He II λ1640[a]	<21.8	<5.4	-
O III] λ1661	<9.0	<2.2	-
O III] λ1666	<8.4	<2.1	-
Fe II λ1786	23.7 ± 5.6	5.7 ± 1.4	-
[C III] λ1907	<10.3	<2.9	-
C III] λ1909	<10.7	<3.0	-
[Ne IV] λ2422	<25.4	<8.8	-
[Ne IV] λ2424	<25.4	<8.8	-
Mg II λ2800[a]	<42.5	<13.0	-
[Ne V] λ3427	<19.0	<11.9	-

Note—Fluxes are not corrected for gravitational magnification. We show 3σ upper limits for non-detections.
[a]: Upper limits (3σ) of line flux and EW of broad permitted, He II, and Mg II emission, assuming FWHM $\simeq2600$ km s^{-1}.
[b]: Total line flux and EW of the C IV $\lambda\lambda$1548, 1551 doublet.

3.1.1. *Lya Emission*

We measure a total Lyα EW of 113 ± 5 Å, consistent with that measured from the R100 prism spectrum (L. J. Furtak et al. 2024; X. Ji et al. 2025). With the SPURS R1000 spectrum, we characterize the Lyα velocity profile (i.e., peak velocity offset, line width). We find that the line profile is asymmetric, with a sharp cutoff near the line center, as expected if the blue Lyα emission is strongly attenuated by the partially neutral IGM at $z\simeq7$ (e.g., M. Dijkstra et al. 2007; A. Saxena et al. 2024; M. Tang et al. 2024b).

The red side of the Lyα profile is very broad. In particular, we find a red tail of emission extending to $\simeq2500$ km s^{-1} from the systemic redshift. This is near-identical to the width of the red-side wing of the broad Hα line which we illustrate in the left panel of Figure 7. The broad component of Lyα appears superimposed on a narrower component peaking closer to line center. To obtain a first-order empirical description of the Lyα emission, we begin by fitting the line profile with two truncated Gaussian functions (e.g., R. Endsley & D. P. Stark 2022), as shown in the right panel of Figure 7. We derive a FWHM of 333 ± 48 km s^{-1} for the narrow component, comparable to the instrument resolution ($\simeq300$ km s^{-1}) and centered at $+258\pm92$ km s^{-1}. The broad component has a FWHM of 1498 ± 145 km s^{-1}, with its peak flux further redshifted (velocity offset $=+1015\pm92$ km s^{-1}).

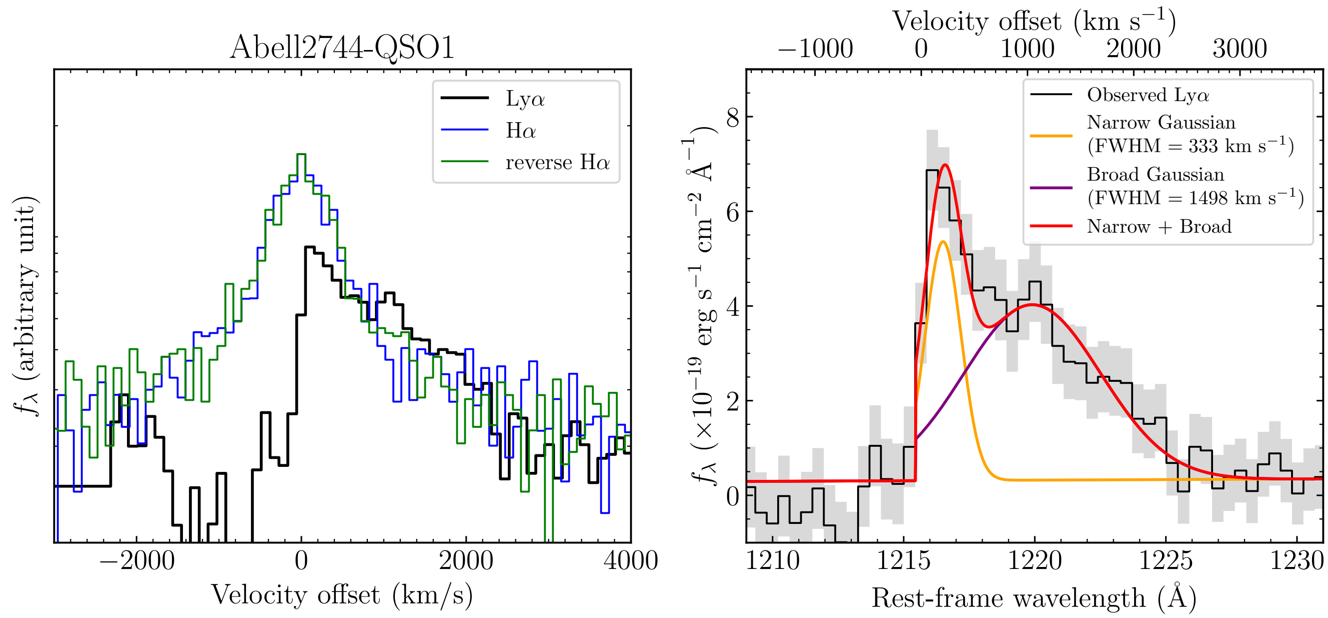

Figure 7. Lyα emission line profile of Abell2744-QSO1. In the left panel, we show Lyα (black) in the velocity space, overplotting the Hα profile (blue) and its reversed velocity profile (green). Both the Lyα and Hα lines are normalized by the flux densities at velocities $2000 - 2500$ km s^{-1} redshifted from the line center. To better compare the wing profiles of Lyα and Hα emission, the flux density (y-axis) is shown in logarithmic scale. In the right panel, we show the empirical two truncated Gaussian fitting (red) to the observed Lyα profile (black). The Lyα can be naively fitted by a narrow (FWHM = 333 km s^{-1}; orange) and a broad (FWHM = 1498 km s^{-1}; purple) component. We will discuss the Lyα profile in more detail in Section 4.

Prior to the SPURS observations, one possibility was that Lyα in Abell2744-QSO1 was entirely associated with ionized gas in the host galaxy. In this case, we would have expected a narrow line profile, similar to that seen in other faint star forming galaxies at high redshift. In Figure 8, we show the Lyα FWHM as a function of absolute UV magnitude for a compilation of high redshift galaxies. For extremely low luminosity hosts like Abell2744-QSO1, we expect the Lyα FWHM to be at most a few hundred km s^{-1}. It is clear that Abell2744-QSO1 has a much broader Lyα line than expected, with FWHM $5 - 10\times$ larger than that of galaxies with similar UV luminosities at $z > 6$. This analysis suggests that there is likely a non-host component associated with the Lyα emission. Or if Lyα is from the host, it must be very different than typical star forming systems. Perhaps a more natural interpretation is that the broad Lyα is linked to whatever mechanism is producing the broad Balmer lines. We will come back to discuss the Lyα profile of Abell2744-QSO1 in more detail in Section 4.

We can estimate the escape fraction ($f_{\rm esc,Ly\alpha}$) of both the narrow and broad components of Lyα using the (dust-corrected) Hα lines to predict the intrinsic Lyα luminosity ($L^{\rm int}_{\rm Ly\alpha} = 8.7 \times L_{\rm H\alpha}$; e.g., E. M. Hu et al. 1998; M. Hayes 2015; A. Henry et al. 2015). As we will note below, such estimates face a range of uncertainties, but they nevertheless will help guide possible explanations for the origin of the line emission. We first focus on the escape fraction of the narrow Lyα line, which we may assume is the host galaxy component. We measure a narrow Lyα line flux of $8.5 \pm 0.8 \times 10^{-19}$ erg s^{-1} cm^{-2} using the decomposition described above. Assuming the Small Magellanic Cloud (SMC) extinction law (K. D. Gordon et al. 2003) and case B recombination (intrinsic Hα/Hβ ratio = 2.87; D. E. Osterbrock & G. J. Ferland 2006), the observed narrow Hα/Hβ ratio (3.9 ± 1.7; Table B2) implies an attenuation of $A_{\rm H\alpha,n} = 0.7 \pm 0.3$ mag to the narrow Hα line. We then derive an escape fraction of 0.086 ± 0.026 for the narrow Lyα line. If we instead assume no attenuation, our results suggest an escape fraction of 0.16 ± 0.05. In both cases, this calculation indicates the bulk of the narrow Lyα line photons are not entering the NIRSpec microshutter. This is common in $z > 7$ galaxies, owing in part to IGM attenuation.

We can follow the same approach for the broad component of Lyα. Our decomposition suggests a broad line flux of $3.2 \pm 0.2 \times 10^{-18}$ erg s^{-1} cm^{-2}. To estimate the escape fraction of broad Lyα photons, we require a measurement of the broad Balmer line luminosity, which in turn requires constraints on the attenuation facing the broad Balmer lines. This is non-trivial owing to the possibility that the Balmer decrement is impacted by scattering and collisional-excitation (e.g., A. de Graaff et al. 2025b; F. D'Eugenio et al. 2025b; G. P. Nikopoulos et al. 2025; S.-J. Chang et al. 2026). If we assume the SMC law and an intrinsic broad Hα/Hβ ratio of 3.06 (X. Dong et al. 2008) that is adopted in previous studies (F. D'Eugenio et al. 2025a; X. Ji et al. 2025), we find an attenuation of $A_{\mathrm{H}\alpha,\mathrm{b}} = 1.8 \pm 0.6$ mag to the broad Hα line using the broad Hα/Hβ ratio (7.0 ± 2.3; Table B2). However, as we noted above, it is possible that the Balmer decrement does not reflect dust attenuation, so we also consider the case where the broad lines do not face attenuation. To predict the intrinsic Lyα luminosity, we furthermore assume case B recombination, which introduces more uncertainty. In the case of modest dust attenuation, we find the broad line region has a Lyα escape fraction of 0.007 ± 0.002. If the broad line attenuation is zero, the inferred broad Lyα escape fraction is 0.034 ± 0.009. In both cases, we find that the observed broad Lyα photons are likely a small fraction of the intrinsic line output.

Finally, we consider the possibility that the entire Lyα profile (narrow and broad components) has its origin in the same gas that produces the narrow Balmer line. This may be expected if the origin of the Lyα emission is not related to the broad Balmer lines, but instead is powered by ionizing sources in the host galaxy. Here we estimate a Lyα escape fraction of 0.75 ± 0.21 assuming no dust attenuation and 0.41 ± 0.12 in the case of modest attenuation implied by the narrow line Balmer decrement.

3.1.2. *High Ionization Lines and Broad Emission Lines*

The SPURS dataset provides our most stringent constraints on high ionization lines in Abell2744-QSO1. The detection of C IV emission suggests the presence of a hard radiation field, supplying ionizing photons with energies > 48 eV. We measure a total C IV flux of $2.5 \pm 0.6 \times 10^{-19}$ erg s^{-1} cm^{-2}, indicating an EW of 5.7 ± 1.3 Å. Such narrow line C IV EWs are commonly seen in metal poor star forming galaxies (e.g., D. A. Berg et al. 2019; P. Senchyna et al. 2019; M. W. Topping et al. 2025).

Given the presence of broad Balmer and Lyα emission lines in the spectrum of Abell2744-QSO1, we may naively expect the permitted C IV emission to show a broad component as well. At the S/N (= 4) of the detected emission, we cannot unambiguously resolve the doublet. We measure a FWHM of 906 km s^{-1} for the C IV emission feature, which is $\simeq 3\times$ narrower than the widths of broad Balmer lines ($\mathrm{FWHM}_{\mathrm{H}\alpha,\mathrm{broad}} = 2653 \pm 345$ km s^{-1}). On the other hand, the observed C IV profile is fully consistent with a blended narrow C IV $\lambda1548, 1551$ doublet whose individual components

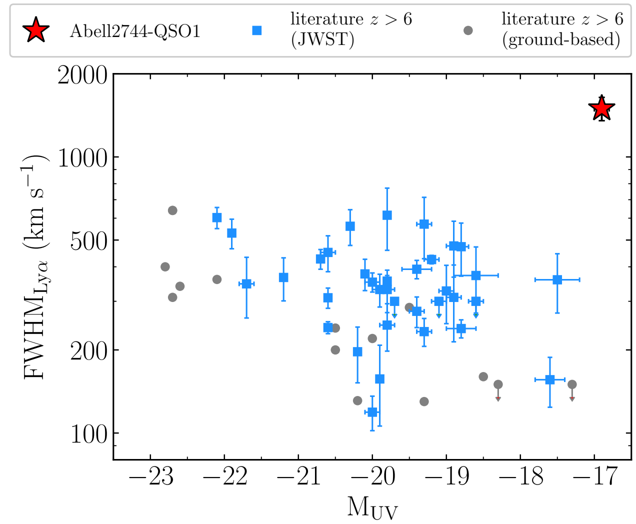

Figure 8. Lyα FWHM versus M$_{\mathrm{UV}}$ of $z > 6$ galaxies. The red star represents Abell2744-QSO1. As a comparison, we overplot data from literature. The cyan squares show systems with Lyα FWHM measured from JWST/NIRSpec R1000 or R2700 grating spectra (A. J. Bunker et al. 2023; M. Tang et al. 2024b; Z. Chen et al. 2025; L. Whitler et al. 2025; J. Witstok et al. 2025). The grey circles show galaxies observed from ground-based facilities (see R. Endsley et al. 2022 and references therein). The Lyα line of Abell2744-QSO1 is much broader than that of other galaxies at similar M$_{\mathrm{UV}}$.

have FWHMs comparable to the instrument resolution. Under the assumption that the detected C IV is associated with the narrow line spectrum, we place an upper limit on the broad C IV emission line flux of Abell2744-QSO1 assuming a $\mathrm{FWHM}_{\mathrm{broad}}$ of 2600 km s^{-1} and integrating the error spectrum in quadrature with a spectral window spanning $2 \times \mathrm{FWHM}_{\mathrm{broad}}$. This implies a 3σ limiting flux of $< 2.3 \times 10^{-19}$ erg s^{-1} cm^{-2}, indicating a broad C IV/Hβ flux ratio of < 0.15. This is well below the typical C IV/Hβ flux ratio of type I AGN (~ 3; e.g., P. J. Francis et al. 1991; M. S. Brotherton et al. 2001; D. E. Vanden Berk et al. 2001).

We also constrain the permitted He II $\lambda1640$ and Mg II lines, both of which could also plausibly be produced in the same line emitting region as the broad Balmer lines. However, we do not detect either broad feature in the SPURS spectrum. Following the same approach as we followed for constraining the broad C IV emission, we place a 3σ limiting flux of $< 2.2 \times 10^{-19}$ erg s^{-1} cm^{-2} to the broad He II emission. This indicates a broad He II/Hβ flux ratio of < 0.14, below that which is typical of type I AGN (~ 0.5; e.g., P. J. Francis et al. 1991; M. S. Brotherton et al. 2001). For the broad Mg II emission, we derive a 3σ limiting flux of $< 4.3 \times 10^{-19}$ erg s^{-1} cm^{-2}. The corresponding broad

Mg II/Hβ flux ratio is < 0.28, more than 5 times lower than that seen in typical type I AGN ($\sim 1.3 - 1.7$; e.g., P. J. Francis et al. 1991; M. S. Brotherton et al. 2001; D. E. Vanden Berk et al. 2001). While Abell2744-QSO1 appears able to produce an emergent broad Lyα line, the other permitted broad lines in the rest-frame UV are not seen.

As the presence of narrow C IV emission reveals a hard radiation field Abell2744-QSO1, we may expect to detect line emission from other highly-ionized species. The G140M spectrum covers N IV], O III], and C III], all emission lines that are seen in metal poor galaxy spectra, particularly those also showing C IV emission. However none of these lines are detected. For the above forbidden lines, we constrain the line flux of each individual component assuming a narrow line (i.e., FWHM is comparable to the instrument resolution, 300 km s^{-1}). The limits are listed in Table 1. In particular, we place a 3σ limiting flux of $< 1.0 \times 10^{-19}$ erg s^{-1} cm^{-2} for each component of the C III] doublet, indicating a line EW that is below 3 Å. Comparing with the C IV detection, the C III]/C IV flux ratio is below 0.8 at 3σ, consistent with photoionization models driven by either massive stars or AGN (e.g., J. Gutkin et al. 2016; A. Feltre et al. 2016; M. Mignoli et al. 2019; A. Plat et al. 2019). We additionally constrain the line flux of the narrow He II emission, placing a 3σ limit of $< 9.2 \times 10^{-20}$ erg s^{-1} cm^{-2}. This indicates a C IV/He II flux ratio of > 2.8 at 3σ, consistent with photoionization models driven by massive stars (e.g., J. Gutkin et al. 2016; A. Feltre et al. 2016).

Finally, we also do not identify higher ionization potential lines (N V, [Ne IV], [Ne V]) for Abell2744-QSO1. With the G140M spectrum, we place a 3σ limiting EW of $<$ 4 Å for each of the individual components of the N V doublet. At the redshift of Abell2744-QSO1, [Ne IV] $\lambda\lambda 2422, 2424$ and [Ne V] $\lambda 3427$ emission lines will be shifted to the G235M spectrum. Our results suggest that each individual component of [Ne IV] ([Ne V]) has an EW below 9 Å (12 Å) at 3σ. The EW limits are similar to those measured from the small number of LRDs with the deepest rest-frame UV grating coverage (e.g., M. Tang et al. 2025b). Given that there are not clear signatures of AGN photoionization in Abell2744-QSO1, we suggest that the narrow C IV emission is plausibly associated with a low metallicity massive stellar population in the host galaxy, as would be expected based on the low metallicities implied by the weak [O III] emission. However, we cannot rule out an association with the LRD.

3.1.3. *O I and Fe II Emission*

O I and Fe II emission lines are often present in the spectra of AGN (e.g., S. A. Grandi 1980; B. J. Wills et al. 1985; A. Rodríguez-Ardila et al. 2002; I. Juodžbalis et al. 2024; R. Tripodi et al. 2025; A. Torralba et al. 2026a). However, these lines have not been reported for Abell2744-QSO1 in previous papers. Because of the similarity of the Lyβ resonance wavelength and that of the 3d^3 D^0 excited state of the O I atom, the strength of O I can be enhanced significantly by Lyβ fluorescence (J. Kwan & J. H. Krolik 1981). We detect O I $\lambda 1302$ emission in the G140M spectrum of Abell2744-QSO1 with a line EW of 3.6 ± 1.1 Å, which may be boosted by Lyβ fluorescence in extremely dense gas. Similarly, the Fe II emission can be enhanced by Lyα fluorescence. We derive an Fe II $\lambda 1786$ EW of 5.7 ± 1.4 Å, stronger than that of typical type I AGN (e.g., D. E. Vanden Berk et al. 2001). These detections suggest that Lyα and Lyβ must be highly optically thick, perhaps consistent with the low Lyα escape fractions described above.

3.1.4. *UV Continuum Slope and Absorption Lines*

In addition to emission lines, the rest-frame UV continuum of Abell2744-QSO1 is marginally detected (median S/N = 2 per resolution element) in the SPURS spectrum, allowing us to quantify the UV slope and constrain the interstellar as well as stellar absorption features. We measure a relatively blue UV continuum slope of $\beta_{\rm UV} = -1.5 \pm 0.3$, consistent with that inferred from NIRSpec prism spectrum ($\beta_{\rm UV} = -1.5$) and NIRCam (M. J. Rieke et al. 2023) broadband photometry ($\beta_{\rm UV} = -1.6$; L. J. Furtak et al. 2023a, 2024).

Depending on the nature of the sources dominating the UV continuum, we may expect to see absorption lines from interstellar gas and massive stars. We first visually search the G140M spectrum for rest-frame UV interstellar absorption lines (Si II $\lambda 1260$, O I $\lambda 1302$, C II $\lambda 1334$, Si IV $\lambda\lambda 1393, 1402$, Si II $\lambda 1526$, C IV $\lambda 1549$, Al II $\lambda 1670$), but none of them are detected. Here we note that because O I and C IV emission is present, the underlying absorption components might be filled in by emission. We constrain the strength of UV interstellar absorption features, placing a 3σ upper limit on EW of $\simeq -2.7$ Å for each individual line. This is consistent with the interstellar absorption line EW measured from composite spectra of galaxies at $z \sim 3 - 7$ (-2 to -1 Å; e.g., A. E. Shapley et al. 2003; T. Jones et al. 2012; C. C. Steidel et al. 2016; A. J. Pahl et al. 2020; K. S. Glazer et al. 2025). Based on these results, our spectrum suggests that interstellar lines are likely somewhat weak in Abell2744-QSO1, which is perhaps not surprising given the low gas covering fractions which are typical at $z > 7$

(K. S. Glazer et al. 2025) and the extremely low metallicity of the host.

Stellar absorption features would provide the most reliable signature that the host galaxy dominates the UV continuum. We search for wind and photospheric absorption features (N V, 1302 index, 1370 index, 1425 index, C IV, 1978 index; S. A. Rix et al. 2004; C. C. Steidel et al. 2016; A. Vidal-García et al. 2017). Neither is clearly detected in the G140M spectrum. However, we note that the limits on photospheric absorption are not sufficiently constraining. Future observations with deeper spectroscopy are required to put more robust constraints on the rest-frame UV absorption features of Abell2744-QSO1.

3.2. *UNCOVER-2476*

We characterize the rest-frame UV spectrum of UNCOVER-2476, which is partially covered by G140M (rest-frame 1930 − 3500 Å) in the SPURS observations. Using the systemic redshift ($z_{\rm sys} = 4.0197$, Section 2.2.2), we visually search the G140M spectrum (Figure 3) for emission lines. The most prominent rest-frame UV line detection is at 14039 Å (S/N = 8) with a companion at 14074 Å (S/N = 3), close to the expected wavelengths of Mg II $\lambda\lambda2796, 2803$ doublet. We identify two iron emission lines [Fe IV] $\lambda2829$ (S/N = 4) and [Fe IV] $\lambda2835$ (S/N = 6). We additionally detect an emission feature at 12169 Å (S/N = 4), consistent with the expected position of [Ne IV] $\lambda\lambda2422, 2424$. Helium emission lines at rest-frame near-UV are also detected, including He II $\lambda2733$ (S/N = 4), He I $\lambda3188$ (S/N = 4), and tentative He II $\lambda3203$ (S/N = 2). We report the rest-frame UV emission line measurements in Table 2. Along with emission lines, the rest-frame UV continuum is clearly present in the G140M spectrum with a median S/N of 6 per resolution element, allowing us to characterize absorption lines. In particular, we find an Fe II $\lambda2586$ absorption feature (S/N = 4), but will also discuss other possible absorption features throughout the rest-frame UV.

3.2.1. *High Ionization Lines*

The detection of [Ne IV] $\lambda\lambda2422, 2424$ emission either points to the presence of a hard radiation field with photons having energies > 64 eV or fast-radiative shocks. As massive stars do not emit many photons at these energies, the former case may require the escape of hard photons from an AGN (e.g., A. Feltre et al. 2016; M. Mignoli et al. 2019; K. Terao et al. 2022). On the other hand, shocks may be expected from dense outflowing and turbulent gas. We measure a total [Ne IV] doublet flux of $1.8 \pm 0.5 \times 10^{-19}$ erg s^{-1} cm^{-2}, corresponding to an EW of 1.3 ± 0.3 Å. The [Ne IV] EW of UNCOVER-2476 is lower than that of other [Ne IV] emission lines identified from JWST/NIRSpec observations (EW $\simeq 10 - 20$ Å; R. Maiolino et al. 2024b; M. Tang et al. 2025b), but such weak lines are common among type I AGN (e.g., P. J. Francis et al. 1991; D. E. Vanden Berk et al. 2001; M. Mignoli et al. 2019). We do not detect emission from more highly ionized neon species ([Ne V]). We place a 3σ limiting flux of $< 1.2 \times 10^{-19}$ erg s^{-1} cm^{-2} on [Ne V] $\lambda3427$ emission, indicating an EW limit < 1.7 Å.

Table 2. Rest-frame UV emission line flux ($\times10^{-20}$ erg s^{-1} cm^{-2}), EW (Å), and FWHM (km s^{-1}) of UNCOVER-2476 measured from SPURS spectra.

Line	Flux	EW	FWHM
[Ne IV][a]	17.9 ± 5.1	1.3 ± 0.3	-
He II $\lambda2733$	18.2 ± 4.4	1.7 ± 0.4	351 ± 85
Mg II $\lambda2796$	28.6 ± 3.8	2.8 ± 0.4	216 ± 75
Mg II $\lambda2803$	11.5 ± 3.6	1.2 ± 0.4	135 ± 75
[Fe IV] $\lambda2829$	12.6 ± 3.3	1.3 ± 0.3	227 ± 74
[Fe IV] $\lambda2835$	21.8 ± 3.7	2.3 ± 0.4	210 ± 74
He I $\lambda3188$	17.3 ± 3.5	2.2 ± 0.5	182 ± 66
He II $\lambda3203$	5.8 ± 2.4	0.7 ± 0.3	118 ± 65
[Ne V] $\lambda3427$	< 12.0	< 1.7	-

Note—Fluxes are not corrected for gravitational magnification. We show 3σ upper limits for non-detections.
[a]: Total line flux and EW of the [Ne IV] $\lambda\lambda2422, 2424$ doublet.

We also find high ionization emission from [Fe IV] and He II in the rest-frame near-UV. Both components of the [Fe IV] $\lambda\lambda2829, 2835$ doublet are narrow, with FWHM ($210 - 227$ km s^{-1}) comparable to the instrument resolution within 1σ uncertainty. Such narrow [Fe IV] emission lines are occasionally found in type II AGN (e.g., M. Rose et al. 2011). The He II $\lambda2733$ emission line is associated with the $n = 6$ to $n = 3$ transition of He$^+$. We derive an EW of 1.7 ± 0.4 Å for He II $\lambda2733$, consistent with the typical EW seen in type II AGN (e.g., N. L. Zakamska et al. 2003).

3.2.2. *Mg II Emission*

The SPURS G140M spectrum reveals narrow Mg II emission lines (FWHM = 135 km s^{-1} for Mg II $\lambda2796$ and 216 km s^{-1} for Mg II $\lambda2803$). We derive an EW of 2.8 ± 0.4 Å for Mg II $\lambda2796$ emission and 1.2 ± 0.4 Å for Mg II $\lambda2803$ emission, comparable to the Mg II EWs measured in the spectra of low-metallicity star-forming galaxies (e.g., N. G. Guseva et al. 2013; Y. I. Izotov et al. 2016, 2018; A. Henry et al. 2018). On the other hand, we do not detect broad Mg II emission. Assuming a line width that is comparable to the broad Balmer emission lines (FWHM = 2000 km s^{-1}; Table A1), we constrain a 3σ limiting flux of $< 3.0 \times 10^{-19}$ erg s^{-1} cm^{-2} for the broad Mg II. This indicates a broad Mg II/Hβ flux ratio of < 0.14, well below the ratios seen in typical type I AGN ($\sim 1.3 - 1.7$; e.g., P. J. Francis et al. 1991; M. S. Brotherton et al. 2001; D. E. Vanden Berk et al. 2001).

The Mg II emission also provides insight into the gas conditions of UNCOVER-2476. The Mg II line fluxes indicate a doublet ratio of $f_{\rm MgII\lambda2796}/f_{\rm MgII\lambda2803} = 2.5 \pm 0.8$. This is close to the intrinsic Mg II doublet ratio (2) when collisions dominate the Mg$^+$ excitation, as expected from optically thin Mg II gas (e.g., J. Chisholm et al. 2020; S.-J. Chang & M. Gronke 2024). We note that the Mg II emission can be pumped, but the Mg II pumping itself should not alter the doublet ratio. We also find that the Mg II velocity offset is small. The flux peak of Mg II λ2796 (Mg II λ2803) is just $+32 \pm 75$ km s^{-1} ($+96 \pm 75$ km s^{-1}) offset from the line center, as expected if Mg$^+$ photons have experienced minimal resonant scattering in optically thin gas. The ionized gas in the narrow-line emitting region (plausibly ionized gas in the host galaxy) appears to be minimally covered by dense neutral gas.

3.2.3. *UV Continuum Slope and Absorption Lines*

The rest-frame UV continuum detection allows us to measure the UV slope. While it is common to derive a UV slope by fitting the continuum spectrum at rest-frame 1250 − 2600 Å (e.g., D. Calzetti et al. 1994), our G140M spectrum only covers rest-frame wavelength > 1930 Å, so we derive the UV slope by fitting the continuum spectrum at rest-frame 1930 − 2600 Å. Nevertheless, we still find a UV slope ($\beta_{\rm UV} = -1.82 \pm 0.03$) that is consistent with the photometric measurement ($\beta_{\rm UV} = -1.76 \pm 0.01$; I. Labbe et al. 2025). This indicates that UNCOVER-2476 has a bluer UV continuum relative to much of the LRD population (median $\beta_{\rm UV} = -1.43$; A. de Graaff et al. 2025b). It is plausible this suggests a more dominant host galaxy contribution to the UV, consistent with the weaker Balmer break.

The high S/N of UV continuum (median S/N = 6 per resolution element) also enables us to constrain the photospheric absorption lines from OB stars, potentially providing insight into the contribution of the host galaxy. One of the most commonly used indices at rest-frame near-UV wavelengths is the 1978 index, which is dominated by iron photospheric lines. We calculate the EW of the 1978 index using the methods in S. A. Rix et al. (2004), getting an EW of -3.6 ± 1.9 Å. This indicates a tentative detection (S/N = 2) of the 1978 index absorption feature, broadly consistent with the EW that is expected from low metallicity stars ($Z = 0.07\ Z_\odot$, see Section A; S. A. Rix et al. 2004). We also detect the Fe II λ2586 absorption line in the continuum spectrum, with Fe II λ2586 EW of -3.2 ± 0.8 Å. This is less prominent than the absorption line EWs of quasars ($\simeq -10$ Å and even stronger; e.g., P. Rodríguez Hidalgo et al. 2011; A. Rafiee et al. 2016; F. D'Eugenio et al. 2025b) but comparable to those that are commonly seen in star-forming galaxies (~ -3 to -1 Å; e.g., A. M. Quider et al. 2009; K. H. R. Rubin et al. 2010; H. Finley et al. 2017).

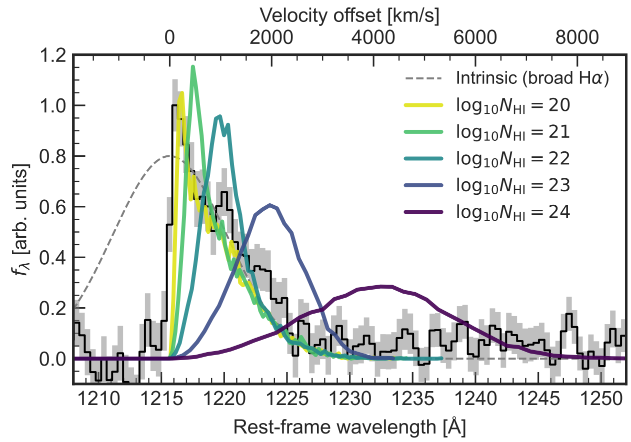

Figure 9. Lyα spectra after resonant scattering through a static uniform shell with a range of H I column densities (colored lines), assuming the intrinsic line profile is similar to the broad component of Hα (FWHM ≈ 2600 km s^{-1}, gray dashed line). We truncate the emergent profiles blueward of systemic velocity, as expected from scattering in the IGM at $z > 6$. We also show the observed Lyα spectrum for comparison (black line). Due to the high cross-section for scattering in the damping wings, gas with $N_{\rm HI} > 10^{21}$ cm^{-2} will be optically thick to photons far from Lyα line center and thus significantly redshift the emerging line shape. The noisiness of the model lines is due to numerical effects.

4. CHARACTERIZING Lyα IN ABELL2744-QSO1

With our G140M spectrum we have characterized the Lyα emission line profile in Abell2744-QSO1, finding it has both a narrow component (FWHM ~ 300 km s^{-1}), centered at ~ 260 km s^{-1} from line center, and an extremely broad component (FWHM ~ 1500 km s^{-1}), offset by ~ 1000 km s^{-1} from line center (Section 3.1), and a sharp cut-off blueward of line center. As a resonant line, the velocity profile of Lyα is extremely sensitive to the properties of the gas through which the photons scatter. In particular, Lyα profiles are strongly shaped by H I column density (T. F. Adams 1972; D. A. Neufeld

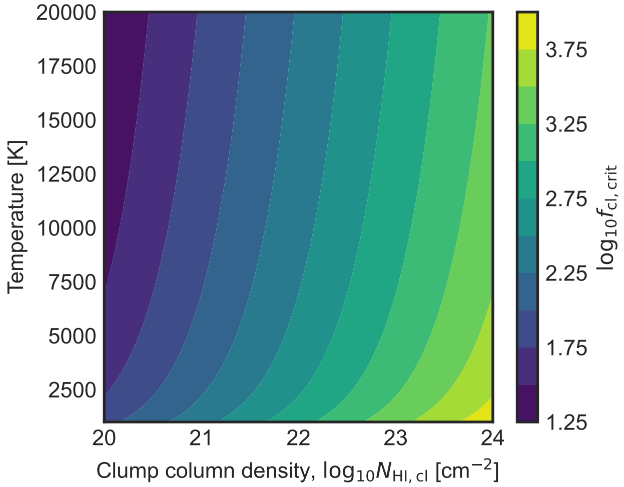

Figure 10. Maximum number of dense gas clumps along the line-of-sight, $f_{\rm cl,crit}$, that would allow broad Lyα to escape without significant redshifting. We show $f_{\rm cl,crit}$ as a function of the clump column density and temperature, following M. Gronke et al. (2017). The large values of $f_{\rm cl,crit}$ imply that there can be a very high covering fraction ($F_{\rm cov} \lesssim 1 - e^{-f_{\rm cl}}$) of dense clumps and some Lyα can still escape without significantly altering the lineshape.

1990; A. Verhamme et al. 2006), as well as dust content (P. Laursen et al. 2009) and gas kinematics (J. R. M. Bonilha et al. 1979; S.-H. Ahn et al. 2002). As described in Section 3.1.1, the Lyα emission in Abell2744-QSO1 is $5 - 10\times$ broader than Lyα emission lines in sources of similar UV luminosities at $z > 6$, implying gas conditions and/or Lyα scattering mechanisms that are not typical of star-forming galaxies. In this section, we investigate the H I gas properties which may explain the Lyα velocity profile in Abell2744-QSO1. We will discuss the implications for the gas environment of LRDs and their host galaxies in Section 5.

In what follows, we consider two possible scenarios for the origin of Lyα and investigate the gas properties implied in each case. We assume flux cut-off blueward of line center is due to scattering in the IGM, as seen ubiquitously in $z \gtrsim 6$ Lyα emission lines (e.g., A. Saxena et al. 2024; M. Tang et al. 2024b) and expected from the high Gunn-Peterson optical depth (J. E. Gunn & B. A. Peterson 1965) at these redshifts (e.g., S. E. I. Bosman et al. 2022; Y. Qin et al. 2025). Thus, we truncate all models blueward of line center when fitting and comparing with the observed profile.

4.1. *Intrinsically Broad Lyα*

Motivated by the similarity between the Lyα and Hα profiles (Figure 7), we first consider a scenario where Lyα and the Balmer lines are produced and broadened to FWHM $\gtrsim 2000$ km s^{-1} in the same region – for example, via Doppler shifting in a BLR and/or Thomson scattering, though we note our spectrum does not reach sufficient S/N to determine if the Lyα shows an exponential wing. In this case, the intrinsic Lyα line profile should be similar to Hα. The broad lines subsequently propagate through dense neutral gas which may imprint absorption in the Balmer lines and continuum ($N_{\rm HI} \sim 10^{24}$ cm^{-2}, e.g., F. D'Eugenio et al. 2025a; X. Ji et al. 2025; R. P. Naidu et al. 2025).

Figure 9 shows the Lyα spectra predicted if an intrinsically broad emission line (FWHM $= 2600$ km s^{-1}, assuming the broad component of Hα, see Table B2) resonantly scatters through a static, uniform shell of gas, assuming different H I column densities and a gas temperature of 10^4 K, using the Monte Carlo radiative transfer code `tlac` (M. Gronke & M. Dijkstra 2014). It is clear that intervening gas with column density $N_{\rm HI} \gtrsim 10^{23}$ cm^{-2}, i.e., as typically required to explain the Balmer break and Balmer line absorption, would significantly alter the observed Lyα spectrum, as it would be extremely optically thick ($\tau > 10^3$) to photons up to ≈ 1000 km s^{-1} redward of line center. In a static, uniform medium, Lyα photons are more likely to escape if they diffuse in frequency/velocity beyond these velocities; thus the profile emerging from such an optically thick medium should be significantly redshifted (e.g., T. F. Adams 1972; D. A. Neufeld 1990). Outflows and/or random motions in the gas can facilitate Lyα escape closer to line center if photons appear redshifted away from the high optical depth in the rest-frame of the gas. However this would require extreme velocities (i.e., > 1000 km s^{-1} if $N_{\rm HI} > 10^{23}$ cm^{-2}), which are not consistent with the $\lesssim 100$ km s^{-1} offsets of the Balmer line absorption features in Abell2744-QSO1 (F. D'Eugenio et al. 2025a). This suggests that, if the intrinsic line profile is broad, the majority of the observed Lyα emission in Abell2744-QSO1 does not scatter through a uniform medium of high column density gas ($N_{\rm HI} > 10^{23}$ cm^{-2}).

In this scenario, the only viable way for Lyα to escape without significant frequency redistribution is if the dense gas is clumpy, embedded in a lower density medium, such that Lyα photons mostly scatter off the surface of dense clumps (D. A. Neufeld 1991; M. Hansen & S. P. Oh 2006). This occurs if Lyα photons are more likely to escape by scattering via random walk *between* clumps than by diffusing in frequency by resonantly scattering *through* clumps. M. Gronke et al. (2016) demonstrated there is a critical number of clumps, $f_{\rm cl,crit}$, along the line-of-sight, above which resonant scattering significantly alters the Lyα line shape. At the high column densities considered here, $N_{\rm HI,cl} \gtrsim$

10^{20} cm^{-2}, even clumps with large random velocities will be optically thick to photons emitted at Lyα line center (i.e., $\tau_{\mathrm{Ly}\alpha}(v_{\mathrm{cl}}) > 1$, even if $v_{\mathrm{cl}} \approx 1000$ km s^{-1}). In this case, the critical number of clumps is a function of the clump H I column density, $N_{\mathrm{HI,cl}}$, and temperature: $f_{\mathrm{cl,crit}} \approx (N_{\mathrm{HI,cl}}/10^{17}\,\mathrm{cm}^{-2})^{1/2}(T/10^4\,\mathrm{K})^{-1}$ (essentially the static case described by M. Gronke et al. 2017, see their Equation 9). If the number of clumps along the line of sight $f_{\mathrm{cl}} < f_{\mathrm{cl,crit}}$, it is possible for some Lyα photons to escape with little resonant scattering and there is no significant change in the intrinsic line shape. The angular covering fraction of clumps can be estimated assuming an isotropic Poisson distribution of clumps: $F_{\mathrm{cov}} = 1 - e^{-f_{\mathrm{cl}}}$. Consequently, even a medium with a near unity covering fraction is effectively 'porous' to Lyα, providing the number of clumps per sightline is below $f_{\mathrm{cl,crit}}$.

Figure 10 shows $f_{\mathrm{cl,crit}}$ as a function of the clump H I column density and gas temperature. We show the range of H I ($n = 1$) column densities required to produce Balmer line absorption, providing the $n = 2$ population is boosted by collisional excitation ($n_2/n_1 \sim 10^{-6}$), and temperatures which have been suggested for the neutral envelopes of LRDs ($\sim 2000 - 2\times10^4$ K; e.g., A. de Graaff et al. 2025b). Given these high column densities, we find the maximum covering fraction of clumps could be up to almost unity (e.g., $f_{\mathrm{cl,crit}} \approx 15$ for $N_{\mathrm{HI,cl}} = 10^{20}$ cm^{-2}), and the Lyα line shape could still be preserved. Increasing the column density raises $f_{\mathrm{cl,crit}}$, and correspondingly, the maximum covering fraction before which the line profile will change, as photons preferentially escape via a random walk reflecting off optically thick clumps rather than scattering through them. Conversely, higher gas temperatures at fixed $N_{\mathrm{HI,cl}}$ decrease $f_{\mathrm{cl,crit}}$ as the clump optical depth is reduced via Doppler broadening. While derived for Lyα photons close to line center, these conclusions should hold for photons at higher velocities, as the timescale for escape via reflections remains significantly shorter than escape via scattering in very optically thick clumps (M. Gronke et al. 2017). Future dedicated radiative transfer simulations will be important for understanding the impact of such dense clumps on the extended wings of Lyα. Overall, this implies that the Lyα profile can be compatible with high H I column densities, provided the gas is clumpy, and that the clumps could have a high angular covering fraction.

Our detections of permitted Fe II and O I UV lines in Abell2744-QSO1 provide additional evidence for a clumpy medium, and are important for reconciling the Lyα profile with the low Lyα escape fraction ($< 10\%$). These transitions are likely excited via Lyα/Lyβ pumping in optically thick gas (J. Kwan & J. H. Krolik 1981; T. A. A. Sigut & A. K. Pradhan 2003). In a clumpy medium, Lyα (and Lyβ) photons will scatter in the surface of optically thick clumps before escaping (D. A. Neufeld 1991; M. Hansen & S. P. Oh 2006), providing a channel for Lyα destruction via fluorescence – explaining the low $f_{\mathrm{esc,Ly}\alpha}$ – while simultaneously providing a mechanism to pump the H I $n = 2$ population required for Balmer line absorption. The profiles of these lines also help to localize the clumps. The narrow widths of the Fe II and O I lines (~ 300 km s^{-1}) and the similarity between Lyα and Hα profiles imply the clumps are in a lower velocity, low optical depth (τ_e) outer region of the LRD compared to the broad line emitting region[22]. Deeper grating spectroscopy of the extended wings of these lines would help to further constrain the location of the clumps.

If dust is present around the LRD and the majority of the dust is in dense clumps, Lyα photons could pass through the medium without significant dust absorption (D. A. Neufeld 1991; P. Laursen et al. 2013; M. Gronke et al. 2017), while the Balmer lines, and other permitted lines with lower cross-sections than Lyα, would propagate through the clumps and be partially absorbed by dust as they experience a higher dust optical depth. If this is the case for Abell2744-QSO1, the observed Lyα escape fraction would be larger than expected from the broad line dust attenuation. Assuming the SMC extinction law (K. D. Gordon et al. 2003), the broad line attenuation $A_{\mathrm{H}\alpha,\mathrm{b}} = 1.8 \pm 0.6$ mag derived from the Balmer decrement (Section 3.1.1) corresponds to a Lyα escape fraction due to dust absorption of $f_{\mathrm{esc,Ly}\alpha} \sim e^{-\tau_{\mathrm{dust}}} < 0.02\%$ (e.g., A. Verhamme et al. 2006). This is over an order of magnitude lower than the Lyα escape fraction we estimated for the broad component ($0.7 \pm 0.2\%$). If the Balmer decrement is mostly due to dust attenuation, this implies that Lyα photons are less attenuated than the Balmer lines, with a clumpy medium providing a potential explanation for the higher than predicted escape fraction. As noted in Section 3.1.1, collisional excitation in dense gas may boost the Balmer decrement, and also Lyα flux, which may impact the interpretation of the Lyα escape fractions.

In summary, dense clumps allow the transmission of broad Lyα without significant resonant scattering or dust attenuation. We discuss how such a clumpy medium could self-consistently produce the Balmer break and line absorption in Section 5.

[22] A high τ_e would preferentially broaden the Lyα wings relative to Hα as Lyα photons traverse a longer path length through the medium as they scatter via a random walk off clumps (M. Gronke et al. 2017).

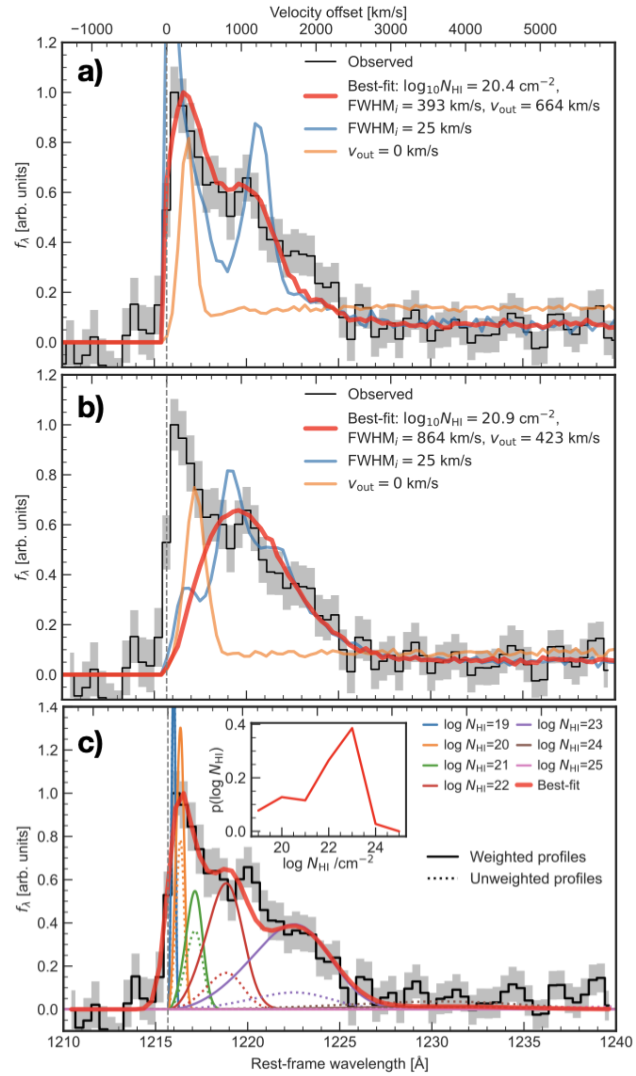

Figure 11. Best-fit Lyα profiles for Abell2744-QSO1 (red lines), compared to the observed profile (black) assuming the profile is shaped by resonant scattering for three cases described in Section 4.2. a) The `zELDA` fit to the full profile which requires high outflow velocities and a high intrinsic linewidth. Reducing the intrinsic FWHM (blue line) or outflow velocity (orange line) cannot reproduce the observed profile. b) The `zELDA` fit to the broad component of the line, which is qualitatively similar to the full profile fit but requires a higher column density. c) Assuming Lyα scatters through an inhomogeneous H I distribution and thus can be described by a weighted sum of profiles at different H I column densities (see Section 4, following S. Almada Monter et al. 2026). Colored lines show the weighted (solid) and unweighted (dashed) profiles at different $N_{\rm HI}$. The inset plot shows the $N_{\rm HI}$ probability distribution function recovered from the best-fit weights.

4.2. *Intrinsically Narrow Lyα*

Alternatively, Lyα may originate from outside of the region where Balmer absorption occurs. For example, in star-forming regions in the host galaxy or in the dense nuclear region around the LRD (e.g., Y. Asada et al. 2026; K. Inayoshi et al. 2026). In this case, the intrinsic Lyα emission would be narrow (broadened only by thermal and turbulent motions in H II regions), and the observed broad profile would arise from resonant scattering in dense gas around the star-forming regions. The similarity between Lyα and Hα in Abell2744-QSO1 would then be coincidental.

We now consider what gas conditions can produce a Lyα profile consistent with Abell2744-QSO1 via resonant scattering. We first fit the profile assuming Lyα scatters through a uniform gas shell with fixed $N_{\rm HI}$, including outflows (e.g., S.-H. Ahn et al. 2002; A. Verhamme et al. 2006). We use the `zELDA` code (S. Gurung-López et al. 2019, 2022), which is built on a large grid of Lyα Monte Carlo radiative transfer simulations, to fit the profile as a function of: the shell column density $N_{\rm HI}$; the outflow velocity, $v_{\rm out}$; dust optical depth $\tau_{\rm dust}$; the intrinsic linewidth (e.g., set by thermal motions in the emitting region); and the intrinsic Lyα EW. We use `zELDA` to fit the observed emission line with an MCMC, using a Gaussian likelihood function. We fit both the full profile, and the broad component (as derived in Section 3.1.1) alone – assuming the narrow component described in Section 3.1.1 is produced outside of the LRD region (we subtract the narrow component, which, with FWHM ≈ 300 km s^{-1} is comparable to Lyα seen in star-forming galaxies; Figure 8). As above, we apply IGM attenuation to the blue side of the model. Our goal is to understand the range of gas properties that would be required to recreate the observed line profile, and we focus here on the inferred kinematics and column density. We show the fitting results in Figure 11.

In both cases, we obtain reasonable fits, but the inferred intrinsic line widths, before scattering, are very broad (FWHM > 300 km s^{-1}), larger than the optical forbidden lines in Abell2744-QSO1 (see Table B2). Fitting the full profile (Figure 11a) requires an intrinsic Lyα linewidth before scattering FWHM$_i \approx 300-400$ km s^{-1} (68% range), and for the Lyα to scatter through gas with moderate column density $N_{\rm HI} \approx 10^{20.5}$ cm^{-2} outflowing[23] at $v_{\rm out} \approx 600-700$ km s^{-1}. Slower outflow velocities would shift the emergent Lyα peak to smaller velocity offsets, while narrower intrinsic lines would produce a profile more sharply peaked than the observed one, because most photons would scatter near line center rather than in the wings. Higher column densities

[23] In this case the secondary red peak stems from "backscattered" Lyα photons, which thus obtain a $\sim 2v_{\rm out}$ frequency boost (A. Verhamme et al. 2006).

would broaden and shift the peak redwards beyond what is observed. Fitting only the broad Lyα component yields similar conclusions (Figure 11b). These fits require an extremely high intrinsic linewidth FWHM$_i \approx 400 - 1200$ km s^{-1}, and scattering through a shell with high outflow velocity $v_{\rm out} \approx 400 - 500$ km s^{-1} and moderate $N_{\rm HI} \approx 10^{20.9}$ cm^{-2}. Such high intrinsic line widths and outflow velocities considerably exceed those inferred from Lyα in $z \sim 3 - 6$ galaxies with similar UV magnitudes to Abell2744-QSO1 (M. Gronke 2017; W. Karman et al. 2017). The requirement for high intrinsic line widths implies highly supersonic turbulence (Mach number $M \gtrsim 50$) that would be unsustainable in homogeneous neutral gas (e.g., M.-M. Mac Low 1999), suggesting that the Lyα emission in Abell2744-QSO1 is not predominantly broadened by resonant scattering in a homogeneous medium.

Alternatively, the Lyα line profile may be explained by resonant scattering through an inhomogeneous gas distribution. Turbulence, which has been suggested to be important for producing smooth Balmer breaks in LRDs (X. Ji et al. 2025; R. P. Naidu et al. 2025), has been shown to drive broad column density distributions in gas clouds (e.g., E. Vázquez-Semadeni et al. 1998; C. Federrath et al. 2010). We fit the observed Lyα profile following S. Almada Monter et al. (2026) who showed Lyα emission from inhomogeneous H I distributions traces the full distribution of H I and can be approximated as a sum of analytic models at a given $N_{\rm HI}$ weighted by $p(\log_{10} N_{\rm HI})$. Thus, we perform a maximum-likelihood fit to the observed profile using a linear combination of analytic models for Lyα emerging from a sphere (M. Dijkstra et al. 2006) to estimate $p(\log_{10} N_{\rm HI})$. We show our best-fit model in Figure 11c, along with the recovered $p(\log_{10} N_{\rm HI})$ distribution. To better understand what drives the recovered $p(\log_{10} N_{\rm HI})$, we also show the individual shell model profiles for a range of $N_{\rm HI}$. We find the majority of the gas needs to be $N_{\rm HI} \sim 10^{22-23}$ cm^{-2} to reproduce the emission at $\sim 1000 - 2000$ km s^{-1}, with a smaller fraction at lower and higher columns: $\sim 30\%$ with $N_{\rm HI} \lesssim 10^{21}$ cm^{-2}, and $< 10\%$ with $N_{\rm HI} \gtrsim 10^{23}$ cm^{-2}, consistent with our discussion of Figure 9. $N_{\rm HI} \sim 10^{22-23}$ cm^{-2} is more than an order of magnitude higher than typical H I column densities inferred for star-forming galaxies with similar UV luminosities to Abell2744-QSO1 at $z \gtrsim 3$ (e.g., N. A. Reddy et al. 2016; K. E. Heintz et al. 2025; C. A. Mason et al. 2026; H. Umeda et al. 2026b). While this implies the broad Lyα is unlikely to come from the surrounding host galaxy, such high column densities could be consistent with a scenario where the Lyα emission is broadened by resonant scattering if it is produced in star-forming regions within a dense, inhomogeneous, nuclear disk (see e.g., Y. Asada et al. 2026; K. Inayoshi et al. 2026).

To summarize, the Lyα profile in Abell2744-QSO1 is unusually broad given its UV magnitude (Figure 8). Given the similarity between the Lyα and Hα profiles, one possibility is that Lyα is produced and broadened in the same region as the Balmer lines. To maintain this similarity, we have shown the observed Lyα photons must primarily escape through $N_{{\rm HI},n=1} < 10^{23}$ cm^{-2} gas, implying the very dense gas responsible for absorption in the Balmer lines cannot fully cover the broad line emitting region. A multiphase medium with dense clumps may allow Lyα to escape without significant frequency distribution or dust attenuation, while still allowing a high covering fraction of dense gas. Alternatively, Lyα could be produced and resonantly scattered outside of the region where the Balmer emission lines and Balmer absorption are produced, i.e., from a star-forming region. In this case, we find the most viable solution to match the line profile requires intrinsically narrow Lyα scattering through an inhomogeneous H I distribution peaking at $N_{\rm HI} \approx 10^{22-23}$ cm^{-2}. While this is over an order of magnitude higher than typical for star-forming galaxies, it could be consistent with dense gas in the nuclear region. Given the similarity of the Lyα and Hα profiles, and that broad Lyα must also be produced along with the broad Balmer lines in the LRD, we consider the former case to be the most likely origin of the Lyα in Abell2744-QSO1. In the next section we will discuss the implications of these results for the geometry of dense gas around LRDs.

5. DISCUSSION

Lyα emission has been detected in many LRDs (Y. Ning et al. 2024; Y. Asada et al. 2026; A. Torralba et al. 2026b), including several at $z > 7$ (L. J. Furtak et al. 2024; G. C. Jones et al. 2026; T. Morishita et al. 2026). However, most interpretation to date of these lines has been limited by the low resolution of NIRSpec prism spectroscopy. Our ultra-deep G140M spectroscopy of Abell2744-QSO1, a $z = 7.04$ LRD, has revealed high EW Lyα emission with a remarkably similar profile to the broad Hα line. This detection is striking on two levels. Firstly, the Lyα profile is incompatible with the high H I column density ($N_{\rm HI} \sim 10^{24}$ cm^{-2}) typically invoked to explain LRDs' Balmer breaks and Balmer absorption features (e.g. A. de Graaff et al. 2025a; K. Inayoshi & R. Maiolino 2025; X. Ji et al. 2025; R. P. Naidu et al. 2025; A. J. Taylor et al. 2025; A. Sneppen et al. 2026): Lyα would be redshifted to > 2000 km s^{-1} to escape such high $N_{\rm HI}$ gas. Secondly, due to the increasingly neutral IGM, at $z > 7$ high EW Lyα ($\gtrsim 100$ Å) is typically only

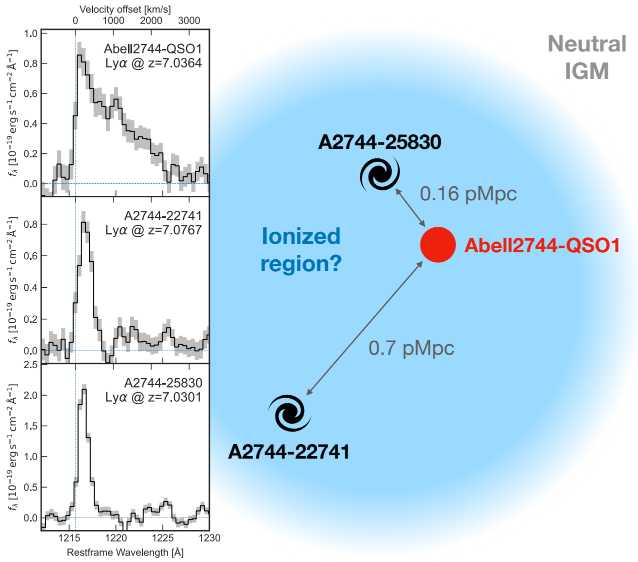

Figure 12. Overview of the three Lyα detections at $z \approx 7.04$ from Abell2744-QSO1, Abell2744-22741 and Abell2744-25830. Finding three strong Lyα emitters in close proximity ($\lesssim 0.7$ pMpc in the source plane) at $z > 7$ suggests they likely reside within an ionized region.

expected from sources in large ionized bubbles (e.g., T.-Y. Lu et al. 2024; M. Tang et al. 2024b; L. Napolitano et al. 2024; Z. Chen et al. 2025). Here we discuss the implications of our results for the environments of LRDs during reionization (Section 5.1) and for the interpretation of dense gas around LRDs (Section 5.2).

5.1. *Ionized Regions around LRDs*

Our deep grating spectroscopy observed Abell2744-QSO1 and its surroundings, providing insights into the environment of an LRD at a redshift where the IGM is mostly neutral (e.g., M. Tang et al. 2024b; Y. Kageura et al. 2025). We spectroscopically confirmed two $z \approx 7.04$ galaxies within 0.68 pMpc (in the source plane) of Abell2744-QSO1, indicating the LRD may trace a dense environment at these redshifts. We illustrate these detections in Figure 12. This is the first evidence that Abell2744-QSO1 has neighbors. Previous spectroscopy in Abell 2744 has been incomplete at this redshift: e.g., at $z > 7$ [O III]+Hβ falls out of the range of the F356W grism used in All the Little Things (ALT, GO 3516, PIs: J. Matthee, R. Naidu; R. P. Naidu et al. 2024), and no other $z = 7.04$ sources were confirmed in UNCOVER MSAs (R. Bezanson et al. 2024). While more complete spectroscopy in Abell 2744 will be needed to verify this, the SPURS detections indicate a significant overdensity. In particular, Abell2744-QSO1 and A2744-25830 are separated by only 0.16 pMpc in the source plane and $\Delta z = 0.0063$. Based on the R. J. Bouwens et al. (2021) $z \approx 7$ UV luminosity function, the expected number of $M_{UV} < -16.9$ galaxies in a cylindrical volume of this scale is just $N \approx 0.02$. This is consistent with recent findings that LRDs preferentially reside in overdense environments: J. Matthee et al. (2025) reported LRDs reside in regions $\sim 6\times$ overdense on ~ 0.1 pMpc scales (see also, e.g., S. Fujimoto et al. 2024; I. Labbe et al. 2024; J.-T. Schindler et al. 2025; T. Morishita et al. 2026).

Most notably, our spectra reveal that both neighboring galaxies also show Lyα emission, as well as signatures of intense radiation fields (Section 2.3). All three sources have Lyα EWs considerably exceeding the median at $z = 6.5 - 8.0$ (≈ 5 Å, M. Tang et al. 2024b). Finding three strong Lyα emitters in close proximity at $z > 7$ is very rare, as the neutral IGM suppresses Lyα unless sources sit in ionized regions (e.g., L. Napolitano et al. 2024; M. Tang et al. 2024b; J. Witstok et al. 2024; Z. Chen et al. 2025; Y. Kageura et al. 2025). Additionally, all three show Lyα emission with flux close to systemic velocity (Figure 12). As the damping wing optical depth from the neutral IGM preferentially attenuates flux close to Lyα line center, this further points to an ionized region around the galaxies (e.g., J. Miralda-Escudé 1998; M. Dijkstra et al. 2007). In particular, the Lyα emission in Abell2744-25830 is offset by only $+123 \pm 92$ km s^{-1}, one of the lowest known offsets at $z > 7$ (A. Saxena et al. 2023; J. Witstok et al. 2024; M. Tang et al. 2024a,c). Detailed analysis would required higher resolution spectroscopy, however, this may indicate the source resides in an ionized region with low residual neutral fraction which may be expected in the presence of hard radiation fields (C. A. Mason & M. Gronke 2020). We obtain an initial estimate of the size of the ionized region, we use the Lyα EW, and 1σ uncertainties, of the three sources to calculate the median fraction of Lyα transmitted through the IGM, relative to $z \sim 5-6$ galaxies, following the approach of M. Tang et al. (2024b), finding $T_{\mathrm{IGM}} > 0.56$ (95% lower limit). We compare this to the fraction of Lyα flux transmitted through along ionized sightlines with a range of sizes, calculated using the IGM damping wing at $z = 7$, following the approaches in (C. A. Mason & M. Gronke 2020; R. Endsley et al. 2022; G. Prieto-Lyon et al. 2023), assuming Gaussian emission lines centered at the velocity offset of the two new Lyα detections. We find this implies an ionized region $\gtrsim 1$ pMpc (R. Endsley et al. 2022; G. Prieto-Lyon et al. 2023), which is comparable to the median sizes of ionized bubbles predicted by simulations at these redshifts (e.g., T.-Y. Lu et al. 2024; M. Neyer et al. 2024). More complete spectroscopy to confirm other $z \approx 7$ sources in this region and measure their Lyα emission will enable improved constraints on the bubble size (e.g., I. Nikolić et al. 2025).

These Lyα detections raise questions regarding the role of LRDs in ionizing their surroundings. The three sources presented here are all UV-faint ($-19 \lesssim M_{\rm UV} \lesssim -17$), and even with optimistic assumptions on ionizing production and escape, star formation in these sources alone would not be sufficient produce such a $R > 1$ pMpc ionized region (e.g., C. A. Mason & M. Gronke 2020). On one hand, it is possible that LRDs simply trace overdensities, as we have noted above. But the Lyα visibility around such faint systems could also be explained if the a system like Abell2744-QSO1 contributed significantly to ionizing its surroundings, potentially in a past (pre-LRD) phase.

To assess whether LRDs preferentially trace ionized regions we estimate the redshift evolution in Lyα visibility (quantified as the fraction of sources with Lyα EW $>$ 25 Å; e.g., D. P. Stark et al. 2011) of LRDs. We measure the Lyα EWs (or 3σ upper limits if non-detection) of 87 LRDs at $z > 4$ with spectra covering Lyα, from the A. de Graaff et al. (2025b) LRD catalog, using the publicly-available prism spectra reduced by DJA (A. de Graaff et al. 2025c; K. E. Heintz et al. 2025). Following the approach in M. Tang et al. (2024b), we derive the Lyα EW distributions of LRDs in two redshift bins: $z = 4-6$ and $z > 6$. We find that the Lyα fractions of LRDs are consistent with no significant evolution between $z = 4-6$ (31^{+6}_{-6}%) and $z > 6$ (24^{+10}_{-8}%), in contrast with a factor of $\sim 2\times$ decrease in the Lyα fraction in star-forming galaxies over the same redshift range (e.g., M. A. Schenker et al. 2014; L. Pentericci et al. 2018; C. A. Mason et al. 2018; M. Nakane et al. 2024; L. Napolitano et al. 2024; M. Tang et al. 2024b).

While more precise population estimates will require larger samples with sensitive grating spectra to measure low EW emission, this result suggests that the Lyα emission of LRDs may be less attenuated by the neutral IGM than typical star forming galaxies, as would be expected if LRDs tend to trace larger ionized regions. Future work to establish the prevalence of Lyα in LRDs and galaxies in their surroundings at $z \gtrsim 7$, relative to regions without LRDs (e.g., Z. Chen et al. 2025), will be essential for assessing their impact on the neutral IGM.

5.2. *Implications for LRD Structure from Deep UV Spectroscopy*

Rest-frame UV grating spectroscopy is now starting to provide new insights into the structure of LRDs and the origin of their UV emission. In particular, spectrally resolving Lyα provides a critical test for the dense gas picture posited to explain LRDs' optical spectra (see also, A. Torralba et al. 2026b). Dense, high $N_{\rm HI}$ gas is required to provide the H I $n = 2$ population necessary to form a strong Balmer break ($N_{{\rm HI},n=2} \gtrsim 10^{17}$ cm^{-2}). However, the Lyα profile we have observed in Abell2744-QSO1 demonstrates that not all photons experience such high H I columns. Reconciling this requires adjustments to the dense gas picture. Motivated by our Lyα results, we discuss two alternative geometries to explain the spectral features of Abell2744-QSO1, and discuss how this may generalize to other LRDs. We illustrate these geometries, relative to a uniform dense gas picture, in Figure 13.

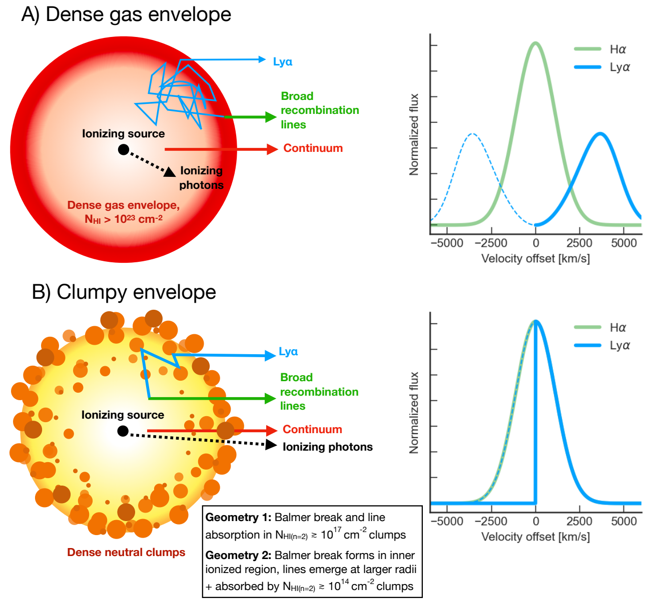

Figure 13. Schematic illustrating the potential geometry of Abell2744-QSO1. A) In a uniform dense gas envelope invoked to form the Balmer break and line absorption in LRDs, Lyα would be extremely redshifted and broadened line relative to Hα (see Section 4.1). B) A high covering fraction of dense neutral clumps around the line emitting region may imprint absorption on the Balmer lines, while some Lyα photons can escape by reflecting off the clumps, preserving the similar Lyα and Hα line profiles.

One natural solution to explain the Lyα is that the dense neutral envelopes invoked for LRDs are clumpy, as we demonstrated in Section 4.1. In this picture (Geometry B1 in Figure 13), the incident continuum and broad emission lines propagate through a layer of dense neutral clumps. Lyα photons escape without significant frequency distribution by scattering off the surfaces of the clumps (e.g., D. A. Neufeld 1991; M. Hansen & S. P. Oh 2006; M. Gronke et al. 2016; S.-J. Chang et al. 2023), while photons with lower H I absorption cross-sections transmit through the clumps, where they can be absorbed by H I in the $n = 2$ state, forming the Balmer break and line absorption. This is similar to a broad line region with a large covering fraction of clouds (K. Inayoshi & R. Maiolino 2025). This interpretation may also help address one of the challenges of the dense gas envelope picture: self-consistently explaining LRDs' smooth reddened Balmer breaks (A. de Graaff et al. 2025c; X. Ji et al. 2025; R. P. Naidu et al. 2025). A radial velocity gradient of clumps in virial motion may help produce a smooth break, by scattering photons at a range of velocities, as has been suggested to explain the exponential-like wings of the emission lines (J. Scholtz et al. 2026). A quantitative analysis of this possibility would require more detailed radiative transfer modeling, accounting for multiphase gas kinematics and Balmer line infilling, and is left for future theoretical work.

Another possibility is that the Balmer break forms *interior* to where the emission lines emerge (Geometry B2 in Figure 13): within the dense, ionized region proposed to explain LRDs' exponential line profiles (S.-J. Chang et al. 2026; V. Rusakov et al. 2026; A. Torralba et al. 2026a). At very high electron densities ($n_e \gtrsim 10^{11}$ cm^{-3}), collisional excitation, as well as Lyα pumping, can boost the H I $n = 2$ population (M. Dijkstra et al. 2016), enabling a Balmer break to form even within highly ionized gas (M. C. Begelman & J. Dexter 2026; Chang et al. in prep; Katz et al. in prep). Motivated by luminous blue variable stars (LBVs) winds (e.g., R. M. Humphreys & K. Davidson 1994), which have been noted to share many spectral features with LRDs (e.g., J. Matthee et al. 2026), a radial density distribution in this ionized region could result in processes occurring in different layers. If the break forms in a dense inner region, extreme electron scattering ($\tau_e \gtrsim 10$) would smooth the entire spectrum, which could naturally explain the smooth, reddened Balmer breaks seen in some LRDs (Katz et al. in prep), and the lack of variability (A. Sneppen et al. 2026), while the observed broad lines emerge from outer, lower-opacity layers ($\tau_e \sim 1-3$, consistent with line profiles in LRDs; J. Matthee et al. 2026; V. Rusakov et al. 2026). To form Balmer line absorption, the line-emitting region is likely surrounded by dense clumps, similar to the previous scenario. Notably, however, this geometry drastically relaxes the $N_{\rm HI}$ requirements for the line absorbing gas. As the Balmer line absorption cross-section is $\sim 10^3\times$ higher than the bound-free cross-section, the line absorbing gas only requires $N_{\rm HI} \gtrsim 10^{20}$ cm^{-2}, which may also facilitate Lyα escape closer to line center. We note column density is a lower limit assuming the $n = 2$ population in this region can also be boosted by collisional excitation and Lyα pumping. This picture could be tested by systematically comparing the $n = 2$ columns inferred from lines versus those from the break in larger LRD samples. A significant implication of this stratified ionized geometry is that if broad line profiles predominantly trace gas kinematics and τ_e at the edge of the line-emitting region, standard virial relations (e.g., J. E. Greene & L. C. Ho 2005; A. E. Reines & M. Volonteri 2015) may introduce additional uncertainties in black hole mass estimates.

While we detected broad Lyα in Abell2744-QSO1, we detected no other broad permitted UV lines (N V, C IV, He II, Mg II). It remains an outstanding question why these lines have been so-far undetected in LRDs (E. Lambrides et al. 2024; M. Tang et al. 2025b), despite being ubiquitous in broad-line AGN at lower redshifts. One possibility, in the context of the stratified ionized geometry discussed above, is that high ionization lines form at radii with high τ_e, and are broadened beyond detectability. It is unclear why the other broad lines would be suppressed in the clumpy envelope picture. A softer ionizing SED than typical AGN could contribute to the lack of broad high ionization lines (e.g., P. Madau & F. Haardt 2024; B. Wang et al. 2025a). However, the non-detection of broad Mg II (ionization potential, I.P. = 7.6 eV) remains particularly puzzling in both scenarios, and we discuss some possible explanations. One possibility is that, as Mg II primarily collisionally excited, it may be intrinsically weak if the required ionization and density conditions to form the line (e.g., K. Korista et al. 1997) exist only in a thin layer. Furthermore, a high $n = 2$ H I population in the gas around the LRD could preferentially absorb Mg II (4.4 eV) relative to Lyα (10.2 eV) via photoionization (I.P. = 3.4 eV for $n = 2$ H I). If the gas around Abell2744-QSO1 is metal poor[24] this would also weaken the Mg II luminosity (see also, R. Maiolino et al. 2025b). Finally, any dust present in the clumps would preferentially attenuate UV metal lines relative to Lyα as the UV lines see a higher dust optical depth through the clumps (D. A. Neufeld 1991; S.-J. Chang & M. Gronke 2024). While Mg II is a resonant line, its optical depth in the clumps is significantly lower than Lyα (e.g., $\sim 10^8\times$ lower given the estimated metallicity of Abell2744-QSO1), making it more likely to scatter through the clumps compared to Lyα (M. Gronke et al. 2017). Comparisons of broad Mg II, if detected, and Lyα lines may thus be a sensitive probe of the clump covering fraction (S.-J. Chang & M. Gronke 2024). Deeper spectroscopy of Mg II in LRDs promises to place stronger limits on broad emission and test these scenarios.

[24] While our Fe II detection indicates metals are present, a high incident Lyα flux may boost the Fe II line strength even at low abundances.

Our detection of a narrow high ionization line, [Ne IV] (I.P. $>$ 64 eV) in UNCOVER-2476 (Section 3.2.1) adds to the sample of such lines detected in LRDs (R. Maiolino et al. 2024b; M. Tang et al. 2025b), potentially implying the presence of radiation fields harder than stellar populations. Whether these high ionization lines indicate AGN photoionization or other sources of hard photons around LRDs remains unclear. Given our results, one possibility is that random motions and outflows of the clumps, potentially aided by radiation pressure from Lyα trapping in their surfaces, may drive clump collisions. Collisions could drive fast radiative shocks capable of powering high ionization lines without a hard incident spectrum (e.g., M. G. Allen et al. 2008; Y. I. Izotov et al. 2012; A. Alarie & L. Drissen 2019). A clumpy medium could also allow the escape of hard continuum photons along low-opacity sightlines in LRDs with non-unity covering fractions (as suggested by E. Lambrides et al. 2025; M. Tang et al. 2025b). While current spectroscopy for most LRDs lacks the depth to detect high ionization UV lines (typical EW $\lesssim$ 10 Å; e.g., J. Chisholm et al. 2024; M. Tang et al. 2025b), ongoing deep grating programs such as SPURS and Deep Insights into UV Spectroscopy at the Epoch of Reionization (DIVER, GO-8018, PI: X. Lin) will enable us to better assess the prevalence and origin of high ionization lines in LRDs.

Of course, the LRDs discussed in this work are only a subset of the population, and whether their diverse spectra can be explained within a unified framework remains to be seen (e.g., A. de Graaff et al. 2025b; P. Madau & R. Maiolino 2026; J. Matthee et al. 2026; W. Q. Sun et al. 2026). Lyα provides a promising probe. $39 \pm 12\%$ of LRDs show Lyα emission in prism spectra (Y. Asada et al. 2026), however only a handful currently have sufficient resolution to measure their line profiles. One question is whether we expect to see broad Lyα in all LRDs if their outer layers are clumpy. T. Morishita et al. (2026) reported broad Lyα in CANUCS-LRD-z8.6, with a line profile similar to Abell2744-QSO1 and also indicative of a large ionized region (though that source does not have a strong Balmer break, R. Tripodi et al. 2025). However, broad Lyα has not yet been reported in other LRDs with high resolution spectra (M. Tang et al. 2025b; A. Torralba et al. 2026b). A range of clump covering fractions around LRDs may naturally explain this diversity: in LRDs with higher clump covering fractions than Abell2744-QSO1, broad Lyα line profiles may be scattered beyond our current detection limits (see A. Torralba et al. 2026b). Higher covering fractions may also favor the production of fluorescent lines and increase Balmer line absorption, a trend that could be tested systematically in larger samples. Furthermore, the detection of broad Lyα in Abell2744-QSO1 may be facilitated by its weak host galaxy contribution: having among the lowest narrow emission line EW (e.g., [O III] λ5007 EW = 5 Å), similar to MoM-BH* (3 Å; R. P. Naidu et al. 2025) and the Cliff (6 Å; A. de Graaff et al. 2025a). In LRDs with a stronger host component, dust within the host galaxy may attenuate some of the broad Lyα flux, a hypothesis that requires a systematic comparison of Lyα emission and inferred dust attenuation.

While rest-frame optical spectra have revealed the extreme densities of LRDs, the rest-frame UV is providing new insights into their potential role in reionization and probes of their structure. Our results suggest LRDs may preferentially reside in large ionized regions, and that the dense gas around them is likely clumpy. Progress will require larger samples with deep UV grating spectroscopy to establish the visibility of Lyα in LRDs and their surroundings during the Epoch of Reionization, and to measure empirical trends between Lyα profiles and LRDs' other spectral features. These observations must be supported by improved radiative transfer simulations of clumpy, high-density environments to help link empirical trends to geometries. Future observations should also be able to detect photospheric lines in UV bright LRDs, providing constraints on the stellar contribution to the UV emission.

6. SUMMARY

We present ultra-deep (29 hours) JWST/NIRSpec G140M (rest-frame UV) spectroscopy of two LRDs in the Abell 2744 field: Abell2744-QSO1 at $z = 7.0364$ and a newly-confirmed LRD UNCOVER-2476 at $z = 4.0197$. The data were obtained as part of the SPURS Cycle 4 Large Program. The deep $R \simeq 1000$ rest-frame UV spectra provide robust constraints on the Lyα velocity profile of Abell2744-QSO1 and high ionization UV emission lines (N V, C IV, He II, [Ne IV], [Ne V]) of these two LRDs. With this dataset, we investigate the gas properties of LRDs and their host galaxies, as well as the galaxy environment that LRDs reside. We summarize our key results below.

1. With deep medium-resolution spectrum, we characterize the Lyα velocity profile of Abell2744-QSO1. The Lyα profile appears to be the superposition of a narrow host-like component (FWHM = 333 km s^{-1}) offset by +258 km s^{-1} from line center, and a broad component (FWHM = 1498 km s^{-1}) offset by +1015 km s^{-1}. The FWHM of broad Lyα is $5 - 10\times$ larger than that of galaxies with similar UV luminosities ($M_{UV} = -16.9$) at $z > 6$, suggesting that the Lyα powering and scatter-

ing mechanisms are not typical of star-forming galaxies. The broad Lyα line width is similar to that of the red-side wing of the broad Hα line, indicating that the broad Lyα may be linked to the mechanism that is producing the broad Balmer lines.

2. We detect narrow C IV emission (EW = 5.7 ± 1.3 Å) in the SPURS G140M spectrum of Abell2744-QSO1. We do not find broad C IV, He II, or Mg II emission. The 3σ upper limits on the ratios between these broad line fluxes and broad Hβ flux are well below that of typical type I AGN. No other very high ionization UV emission line (N V, [Ne IV], [Ne V]) is seen in the spectrum of Abell2744-QSO1. We additionally detect narrow O I λ1302 (EW = 3.6 ± 1.1 Å) and Fe II λ1786 emission (EW = 5.7 ± 1.4 Å). As O I and Fe II can be enhanced by Lyβ and Lyα fluorescence, these detections indicate that some sightlines are highly optically thick to Lyα and Lyβ.

3. The SPURS G140M spectrum of UNCOVER-2476 reveals narrow high ionization emission lines [Ne IV] $\lambda\lambda 2422, 2424$ (EW = 1.3 ± 0.3 Å), He II λ2733, and [Fe IV] $\lambda\lambda 2829, 2835$. This may indicate the presence of hard photons (> 64 eV) which are able to escape along low-opacity sightlines or fast-radiative shocks.

4. We investigate the H I gas properties that can explain the Lyα velocity profile of Abell2744-QSO1. We first consider if Lyα is produced and broadened in the same regions as the broad Balmer lines. If Lyα photons transfer through the very dense neutral gas predicted to be responsible for the Balmer Break ($N_{\rm HI} \sim 10^{24}$ cm^{-2}), the net line profile will be significantly more redshifted and broadened than we observe. We argue that the Lyα profile can be best explained if the dense neutral gas is clumpy. This allows Lyα to escape by scattering off of the clump surfaces without significant resonant scattering or dust attenuation.

5. We newly-identify two close neighbors of Abell2744-QSO1. One of the galaxies (Abell2744-25830) is 0.16 pMpc away and a further source (Abell2744-22741) is 0.68 pMpc away from Abell2744-QSO1 in source plane, both of which also show Lyα emission. These systems appear to suggest that Abell2744-QSO1 traces a dense environment, as is commonly seen in LRDs. The overdensity may carve out an early ionized region, contributing to the boosted Lyα visibility. Future observations are required to test if the the Lyα visibility of LRDs tends to be enhanced owing to the larger-than-average galaxy densities they trace.

ACKNOWLEDGMENTS

MT acknowledges support by a Shanghai Jiao Tong University start-up grant. DPS acknowledges support by the National Science Foundation under Grant No. AST-2109066. CAM acknowledges support by the European Union ERC grant RISES (101163035), Carlsberg Foundation (CF22-1322), and VILLUM FONDEN (37459). ZC acknowledges support by VILLUM FONDEN (37459). The Cosmic Dawn Center (DAWN) is funded by the Danish National Research Foundation under grant DNRF140. MG thanks the Max Planck Society for support through the Max Planck Research Group, and the European Union for support through ERC-2024-STG 101165038 (ReMMU). LJF and RE acknowledge support from the University of Texas at Austin Cosmic Frontier Center. SJC acknowledges support from the ERC synergy grant 101166930 – RECAP. JM acknowledges funding by the European Union (ERC, AGENTS, 101076224). LW acknowledges support from the Gavin Boyle Fellowship at the Kavli Institute for Cosmology, Cambridge and from the Kavli Foundation. AZ acknowledges support by the Israel Science Foundation Grant No. 864/23. VG acknowledges support by the Carlsberg Foundation (CF22-1322).

This work is based on observations made with the NASA/ESA/CSA James Webb Space Telescope. The data were obtained from the Mikulski Archive for Space Telescopes at the Space Telescope Science Institute, which is operated by the Association of Universities for Research in Astronomy, Inc., under NASA contract NAS 5-03127 for JWST. These observations are associated with the program GO 9214. We thank our program coordinator, Christian Soto, and our NIRSpec reviewer, Diane Karakla. The authors acknowledge the UNCOVER team led by Ivo Labbé and Rachel Bezanson for developing their observing programs with zero-exclusive-access periods. Part of the data products presented herein were retrieved from the Dawn JWST Archive (DJA). DJA is an initiative of the Cosmic Dawn Center, which is funded by the Danish National Research Foundation under grant DNRF140. The Tycho supercomputer hosted at the SCIENCE HPC center at the University of Copenhagen was used for supporting this work.

Software: `NumPy` (C. R. Harris et al. 2020), `Matplotlib` (J. D. Hunter 2007), `SciPy` (P. Virtanen et al. 2020), `Astropy` (Astropy Collaboration et al. 2022), `PyNeb` (V. Luridiana et al. 2015), `msaexp` (G. Brammer 2023), `zELDA` code (S. Gurung-López et al. 2019, 2022), `tlac` (M. Gronke & M. Dijkstra 2014)

APPENDIX

A. REST-FRAME OPTICAL AND NIR SPECTRA OF UNCOVER-2476

In this section, we discuss the SPURS rest-frame optical and NIR (G235M and G395M) spectra of UNCOVER-2476 (Figure A1) in more detail. We identify a suite of strong emission lines ([O II], [Ne III], Hγ, Hβ, [O III], Hα; Table A1). We additionally detect several hydrogen (H11, H10, H9, H8, Hϵ, Hδ, Pa10, Pa9, Paϵ, Paδ) and helium (He I λ3889, λ4472, λ5877, λ6680, λ7065, λ7281, λ10830) emission lines. We also find sulfur ([S II] λ6717, S/N = 3; [S II] λ6732, S/N = 1.5; [S III] λ9071, S/N = 5; [S III] λ9533 S/N = 6) and [Ar III] λ7138 (S/N = 3) emission lines. We detect [O III] λ4363 (S/N = 10), [O II] λ7322 (S/N = 2), and [O II] λ7332 (S/N = 2) auroral lines. We also report neutral oxygen lines ([O I] λ6302, S/N = 4; O I λ8446, S/N = 3) and iron emission lines ([Fe II] λ4287, S/N = 3.5; Fe II λ4418, S/N = 3; [Fe VII] λ5159, S/N = 4), which are often seen in type I AGN and LRDs (e.g., F. D'Eugenio et al. 2025b; V. Kokorev et al. 2025; M. Tang et al. 2025b; X. Lin et al. 2026).

Both the Hβ and Hα emission lines show broad and narrow components. We simultaneously fit the narrow and broad Hβ line profile with two Gaussians. We derive FWHMs of 205 $\pm$ 4 km s^{-1} (narrow) and 2123 ± 496 km s^{-1} (broad). The Hα emission line additionally presents an absorption feature, which is shown in a subset of LRDs (e.g., X. Lin et al. 2024; J. Matthee et al. 2024; D. D. Kocevski et al. 2025). We fit the Hα line profile with three Gaussians. For the broad component, we derive a FWHM of 1703 ± 28 km s^{-1}, consistent with the line width of the broad Hβ emission. The Hα absorption line is blueshifted (-257 ± 92 km s^{-1}), with an EW of $= -6.6 \pm 0.9$ Å.

The narrow line detections allow us to characterize the properties of the narrow line emitting gas in UNCOVER-2476. Interpreting the narrow lines requires knowledge of the dust attenuation to these lines, which can be estimated from the Balmer decrement measurement. We measure a narrow Hα/Hβ flux ratio of 3.37 ± 0.19. Assuming the SMC extinction law (K. D. Gordon et al. 2003) and case B recombination (D. E. Osterbrock & G. J. Ferland 2006), we derive a modest narrow line attenuation of $A_V = 0.54 \pm 0.03$ mag. In the following, we will correct the narrow line fluxes with this reddening value.

The strongest narrow line in the spectra of UNCOVER-2476 is [O III] λ5007. We measure an

Table A1. Rest-frame optical and NIR emission line flux ($\times10^{-20}$ erg s^{-1} cm^{-2}), EW (Å), and FWHM (km s^{-1}) of UNCOVER-2476 measured from SPURS spectra.

Line	Flux	EW	FWHM
[O II] λ3727	71.9 ± 7.7	16.4 ± 1.8	162 ± 12
[O II] λ3729	77.7 ± 7.7	17.8 ± 1.8	159 ± 12
H11	23.6 ± 4.2	6.7 ± 1.2	268 ± 62
H10	16.2 ± 3.5	4.3 ± 0.9	217 ± 35
H9	33.6 ± 4.4	8.0 ± 1.0	217 ± 35
[Ne III] λ3869	252.5 ± 7.4	51.3 ± 1.5	183 ± 4
He I λ3889+H8	79.4 ± 7.3	16.6 ± 1.5	-
[Ne III] λ3968+Hϵ	162.5 ± 9.9	38.0 ± 2.3	-
Hδ	230.7 ± 15.5	33.8 ± 2.3	295 ± 14
[Fe II] λ4287	16.6 ± 4.7	3.9 ± 1.1	245 ± 66
Hγ	400.5 ± 18.5	56.9 ± 2.6	275 ± 9
[O III] λ4363	183.7 ± 17.5	26.0 ± 2.5	272 ± 19
Fe II λ4418	25.6 ± 8.8	3.8 ± 1.3	295 ± 112
He I λ4472	41.9 ± 10.3	6.0 ± 1.5	310 ± 76
narrow Hβ	744.5 ± 22.0	91.5 ± 2.7	205 ± 4
broad Hβ	210.1 ± 68.3	25.8 ± 8.4	2123 ± 496
[O III] λ4959	1706 ± 30	208.9 ± 3.7	247 ± 3
[O III] λ5007	5507 ± 44	673.1 ± 5.4	239 ± 1
[Fe VII] λ5159	42.0 ± 10.2	5.5 ± 1.3	229 ± 89
He I λ5877	139.7 ± 11.9	17.2 ± 1.5	218 ± 14
[O I] λ6302	86.3 ± 22.1	9.4 ± 2.4	627 ± 135
narrow Hα	2512 ± 118	221.0 ± 10.4	157 ± 3
broad Hα	4795 ± 165	421.9 ± 14.5	1703 ± 28
He I λ6680	39.3 ± 10.1	3.7 ± 0.9	192 ± 46
[S II] λ6717	36.3 ± 10.9	3.5 ± 1.1	242 ± 69
[S II] λ6732	22.6 ± 14.9	2.2 ± 1.5	170 ± 94
He I λ7065	101.5 ± 14.3	10.7 ± 1.5	270 ± 29
[Ar III] λ7138	41.1 ± 14.0	4.5 ± 1.5	252 ± 64
[O II] λ7322	24.9 ± 11.7	3.0 ± 1.4	-
[O II] λ7332	10.8 ± 5.1	1.3 ± 0.6	-
O I λ8446	45.0 ± 15.4	6.3 ± 2.1	314 ± 67
Pa10	35.2 ± 16.1	4.9 ± 2.2	222 ± 77
[S III] λ9701	62.0 ± 13.2	8.6 ± 1.8	348 ± 125
Pa9	53.5 ± 12.3	7.9 ± 1.8	206 ± 110
[S III] λ9533	156.0 ± 24.7	24.5 ± 3.9	218 ± 27
Paϵ	69.4 ± 15.2	10.9 ± 2.4	199 ± 129
Paδ	133.9 ± 19.3	22.6 ± 3.3	336 ± 79
He I λ10830	530.0 ± 37.5	73.6 ± 5.2	245 ± 18

NOTE—Fluxes are not corrected for gravitational magnification. We show 3σ upper limits for non-detections.

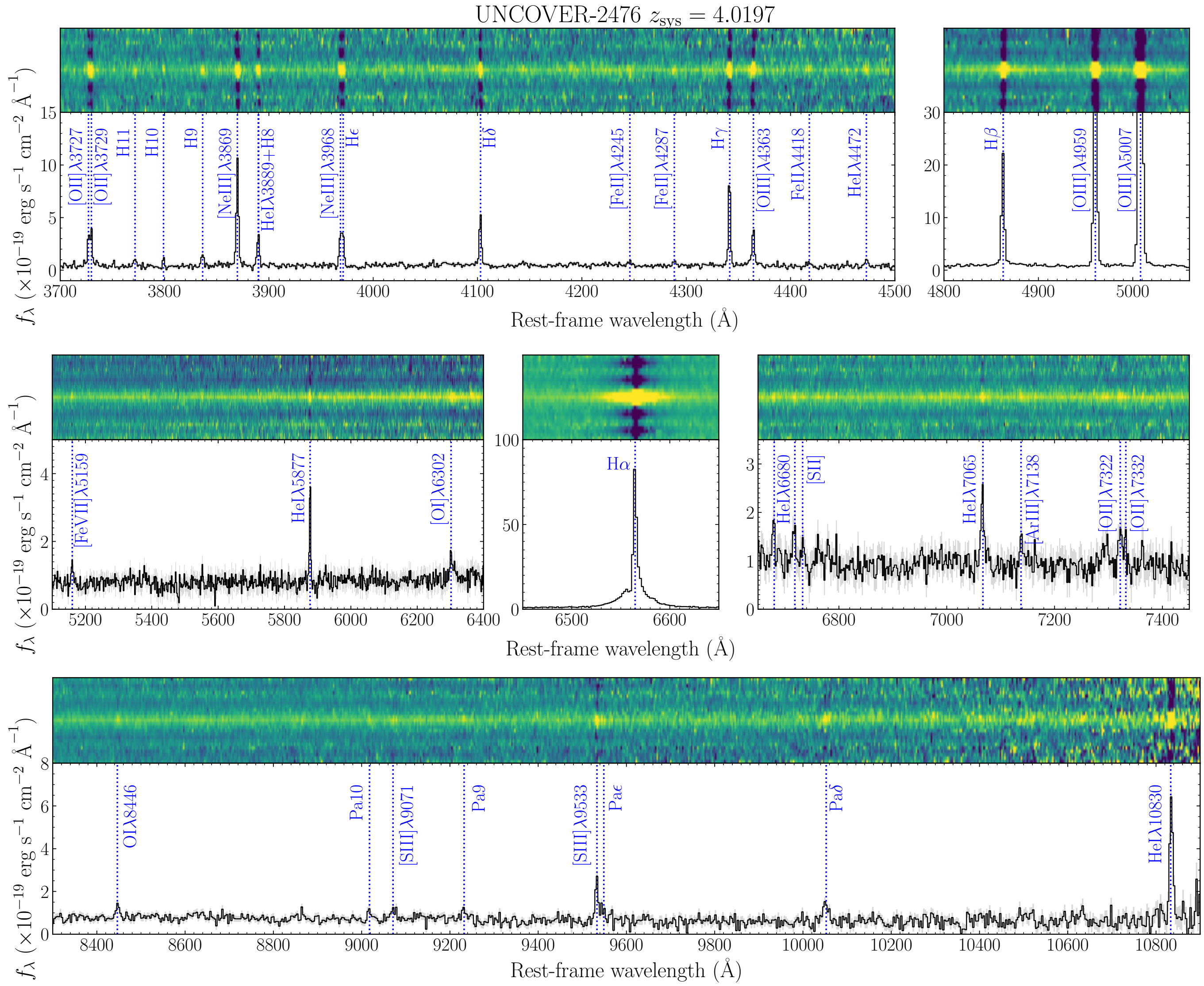

Figure A1. SPURS JWST/NIRSpec rest-frame optical to NIR (G235M/F170LP and G395M/F290LP) spectra of UNCOVER-2476, shown in the same way as Figure 2. We detect broad Hβ and Hα emission lines and several hydrogen and helium lines, as well as a suite of narrow, strong forbidden lines.

[O III] λ5007 flux of $5.51 \pm 0.04 \times 10^{-17}$ erg s^{-1} cm^{-2}, corresponding to an EW of 673 ± 5 Å. Such a large [O III] λ5007 EW is among the upper 10% of the values observed in the LRD population (A. de Graaff et al. 2025b). If the [O III] emission primarily comes from the host galaxy, the large EW would indicate that the galaxy of UNCOVER-2476 is dominated by relatively young stellar populations.

We may expect that the ionization-sensitive line ratios of UNCOVER-2476 are large given the strong [O III] emission (e.g., M. Tang et al. 2019; R. L. Sanders et al. 2020; K. Boyett et al. 2024). We derive a very large [O III]/[O II] (O32) ratio (37 ± 3). This value is more than 10$\times$ of the typical O32 ratio of $z \simeq 4$ star-forming galaxies ($\simeq 3$; e.g., R. L. Sanders et al. 2023; A. E. Shapley et al. 2023), and also 2$\times$ larger than the average O32 measured from the composite spectrum of type I AGN at $z \simeq 4-7$ (19; Y. Isobe et al. 2025). We find a large [Ne III]/[O II] (Ne3O2) ratio as well, reaching Ne3O2 $= 1.7 \pm 0.1$. These suggest that the narrow line emitting gas in UNCOVER-2476 is under extreme ionization conditions.

The detection of auroral lines and [O III] λ4959, 5007, [O II] λ3727, 3729 emission enables us to jointly constrain the electron temperature and density of the narrow line emitting gas. The density-sensitive [O II] λ3727, 3729 doublet is resolved in our G235M spectrum, with a doublet flux ratio of $f_{\rm [OII]\lambda3729}/f_{\rm [OII]\lambda3727} = 1.1 \pm 0.2$. Together with the

Table B2. Rest-frame optical emission line flux ($\times 10^{-20}$ erg s^{-1} cm^{-2}), EW (Å), and FWHM (km s^{-1}) of Abell2744-QSO1 measured from SPURS spectra.

Line	Flux	EW	FWHM
[O II] λ3728	< 35.6	< 20.9	-
[Ne III] λ3869	< 19.0	< 7.6	-
Hγ	< 14.5	< 3.7	-
narrow Hβ	15.8 ± 5.4	3.2 ± 1.1	235 ± 65
broad Hβ	152.9 ± 32.5	31.8 ± 6.8	1674 ± 252
[O III] λ4959	< 16.7	< 3.3	-
[O III] λ5007	25.4 ± 7.9	5.0 ± 1.5	251 ± 80
narrow Hα	61.9 ± 17.4	11.2 ± 3.1	239 ± 48
broad Hα	1069 ± 264	193.1 ± 47.8	2653 ± 345

NOTE—Fluxes are not corrected for gravitational magnification. We show 3σ upper limits for non-detections.

[O II] $\lambda\lambda$7322, 7332 auroral lines and using the PyNeb code (V. Luridiana et al. 2015), we derive a temperature of $T_{\rm e}({\rm O}^+) = 1.9^{+1.1}_{-0.7} \times 10^4$ K and a density of $n_{\rm e} = 470^{+310}_{-220}$ cm^{-3} for the O$^+$ gas. For the O^{2+} gas, we measure a [O III] λ4363/[O III] λ5007 ratio of 0.041 ± 0.004. If the O^{2+} gas has the similar density as the O$^+$ gas, we derive an electron temperature of $T_{\rm e}({\rm O}^{2+}) = 2.2^{+0.1}_{-0.2} \times 10^4$ K. Although note that the O^{2+} gas density may not necessarily be the same as the O$^+$ gas, the temperature of O^{2+} gas does not change significantly with density varying up to $\sim 5 \times 10^4$ cm^{-3}.

Based on the derived oxygen gas temperature and density, we can estimate the gas-phase oxygen abundance of UNCOVER-2476. Using the PyNeb code, we derive $12 + \log{\rm (O/H)} = 7.55^{+0.06}_{-0.05}$ ($Z = 0.07^{+0.01}_{-0.01}\ Z_\odot$, where solar metallicity corresponds to $12 + \log{\rm (O/H)} = 8.71$; J. Gutkin et al. 2016). This is consistent with the average oxygen abundance of high redshift type I AGN inferred from [O III] λ4363 measurement ($12 + \log{\rm (O/H)} = 7.46$; Y. Isobe et al. 2025). The result indicates that the narrow line emitting gas in UNCOVER-2476 is fairly metal poor.

B. REST-FRAME OPTICAL SPECTRA OF ABELL2744-QSO1

We list the rest-frame optical emission line fluxes, EWs, and FWHMs measured from SPURS G395M spectrum of Abell2744-QSO1 in Table B2. The SPURS rest-frame optical spectrum of Abell2744-QSO1 is shown in Figure B2.

REFERENCES

Adams, T. F. 1972, ApJ, 174, 439, doi: 10.1086/151503

Ahn, S.-H., Lee, H.-W., & Lee, H. M. 2002, ApJ, 567, 922, doi: 10.1086/338497

Akins, H. B., Casey, C. M., Lambrides, E., et al. 2025a, ApJ, 991, 37, doi: 10.3847/1538-4357/ade984

Akins, H. B., Casey, C. M., Berg, D. A., et al. 2025b, ApJL, 980, L29, doi: 10.3847/2041-8213/adab76

Alarie, A., & Drissen, L. 2019, MNRAS, 489, 3042, doi: 10.1093/mnras/stz2279

Allen, M. G., Groves, B. A., Dopita, M. A., Sutherland, R. S., & Kewley, L. J. 2008, ApJS, 178, 20, doi: 10.1086/589652

Almada Monter, S., Gronke, M., & Chang, S.-J. 2026, MNRAS, 547, stag330, doi: 10.1093/mnras/stag330

Ananna, T. T., Bogdán, Á., Kovács, O. E., Natarajan, P., & Hickox, R. C. 2024, ApJL, 969, L18, doi: 10.3847/2041-8213/ad5669

Asada, Y., Inayoshi, K., Fei, Q., Fujimoto, S., & Willott, C. 2026, arXiv e-prints, arXiv:2601.10573, doi: 10.48550/arXiv.2601.10573

Astropy Collaboration, Price-Whelan, A. M., Lim, P. L., et al. 2022, ApJ, 935, 167, doi: 10.3847/1538-4357/ac7c74

Begelman, M. C., & Dexter, J. 2026, ApJ, 996, 48, doi: 10.3847/1538-4357/ae274a

Begley, R., McLure, R. J., Cullen, F., et al. 2025, MNRAS, 537, 3245, doi: 10.1093/mnras/staf211

Berg, D. A., Erb, D. K., Henry, R. B. C., Skillman, E. D., & McQuinn, K. B. W. 2019, ApJ, 874, 93, doi: 10.3847/1538-4357/ab020a

Bezanson, R., Labbe, I., Whitaker, K. E., et al. 2024, ApJ, 974, 92, doi: 10.3847/1538-4357/ad66cf

Böker, T., Beck, T. L., Birkmann, S. M., et al. 2023, PASP, 135, 038001, doi: 10.1088/1538-3873/acb846

Bonilha, J. R. M., Ferch, R., Salpeter, E. E., Slater, G., & Noerdlinger, P. D. 1979, ApJ, 233, 649, doi: 10.1086/157426

Bosman, S. E. I., Davies, F. B., Becker, G. D., et al. 2022, MNRAS, 514, 55, doi: 10.1093/mnras/stac1046

Bouwens, R. J., Oesch, P. A., Stefanon, M., et al. 2021, AJ, 162, 47, doi: 10.3847/1538-3881/abf83e

Boyett, K., Bunker, A. J., Curtis-Lake, E., et al. 2024, MNRAS, 535, 1796, doi: 10.1093/mnras/stae2430

Brammer, G. 2023, msaexp: NIRSpec analyis tools, 0.6.17 Zenodo, doi: 10.5281/zenodo.8319596

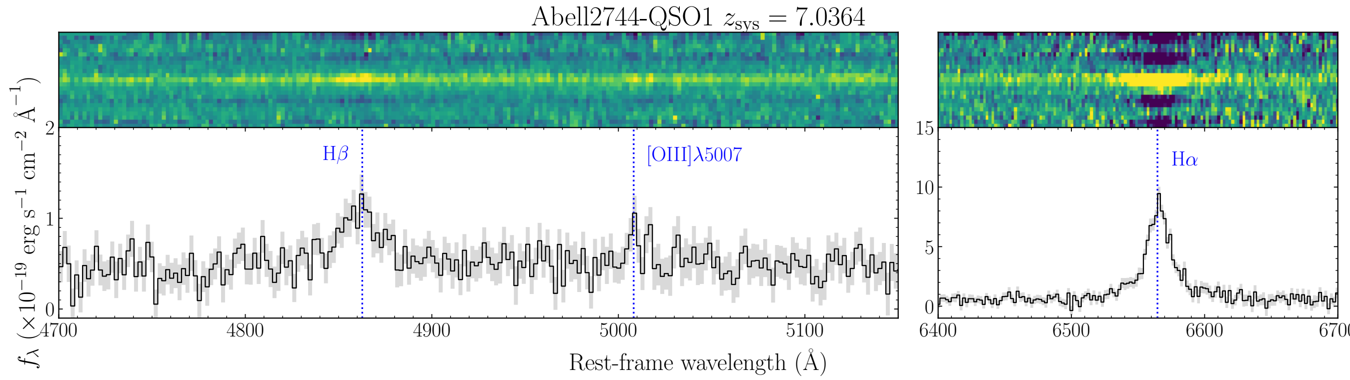

Figure B2. SPURS JWST/NIRSpec rest-frame optical (G395M/F290LP and part of G235M/F170LP) spectra of Abell2744-QSO1, shown in the same way as Figure 2. We detect broad Hβ and Hα emission lines, as well as a narrow, weak [O III] λ5007 emission line.

Brazzini, M., D'Eugenio, F., Maiolino, R., et al. 2025, MNRAS, 544, L167, doi: 10.1093/mnrasl/slaf116

Brotherton, M. S., Tran, H. D., Becker, R. H., et al. 2001, ApJ, 546, 775, doi: 10.1086/318309

Bunker, A. J., Saxena, A., Cameron, A. J., et al. 2023, A&A, 677, A88, doi: 10.1051/0004-6361/202346159

Bushouse, H., Eisenhamer, J., Dencheva, N., et al. 2024, JWST Calibration Pipeline, 1.16.1 Zenodo, doi: 10.5281/zenodo.14153298

Calzetti, D., Kinney, A. L., & Storchi-Bergmann, T. 1994, ApJ, 429, 582, doi: 10.1086/174346

Casey, C. M., Akins, H. B., Finkelstein, S. L., et al. 2025, ApJL, 990, L61, doi: 10.3847/2041-8213/adfa91

Chang, S.-J., & Gronke, M. 2024, MNRAS, 532, 3526, doi: 10.1093/mnras/stae1664

Chang, S.-J., Gronke, M., Matthee, J., & Mason, C. 2026, MNRAS, 545, 1, doi: 10.1093/mnras/staf2131

Chang, S.-J., Yang, Y., Seon, K.-I., Zabludoff, A., & Lee, H.-W. 2023, ApJ, 945, 100, doi: 10.3847/1538-4357/acac98

Chen, Z., Stark, D. P., Mason, C. A., et al. 2025, arXiv e-prints, arXiv:2505.24080, doi: 10.48550/arXiv.2505.24080

Chisholm, J., Prochaska, J. X., Schaerer, D., Gazagnes, S., & Henry, A. 2020, MNRAS, 498, 2554, doi: 10.1093/mnras/staa2470

Chisholm, J., Berg, D. A., Endsley, R., et al. 2024, MNRAS, 534, 2633, doi: 10.1093/mnras/stae2199

Chisholm, J., Berg, D. A., Boylan-Kolchin, M., et al. 2026, arXiv e-prints, arXiv:2602.15935, doi: 10.48550/arXiv.2602.15935

de Graaff, A., Rix, H.-W., Naidu, R. P., et al. 2025a, A&A, 701, A168, doi: 10.1051/0004-6361/202554681

de Graaff, A., Hviding, R. E., Naidu, R. P., et al. 2025b, arXiv e-prints, arXiv:2511.21820, doi: 10.48550/arXiv.2511.21820

de Graaff, A., Brammer, G., Weibel, A., et al. 2025c, A&A, 697, A189, doi: 10.1051/0004-6361/202452186

D'Eugenio, F., Maiolino, R., Perna, M., et al. 2025a, arXiv e-prints, arXiv:2503.11752, doi: 10.48550/arXiv.2503.11752

D'Eugenio, F., Nelson, E., Ji, X., et al. 2025b, arXiv e-prints, arXiv:2510.00101, doi: 10.48550/arXiv.2510.00101

D'Eugenio, F., Juodžbalis, I., Ji, X., et al. 2026, MNRAS, 545, staf2117, doi: 10.1093/mnras/staf2117

Dijkstra, M. 2017, arXiv e-prints, arXiv:1704.03416, doi: 10.48550/arXiv.1704.03416

Dijkstra, M., Haiman, Z., & Spaans, M. 2006, ApJ, 649, 14, doi: 10.1086/506243

Dijkstra, M., Lidz, A., & Wyithe, J. S. B. 2007, MNRAS, 377, 1175, doi: 10.1111/j.1365-2966.2007.11666.x

Dijkstra, M., Sethi, S., & Loeb, A. 2016, ApJ, 820, 10, doi: 10.3847/0004-637X/820/1/10

Dong, X., Wang, T., Wang, J., et al. 2008, MNRAS, 383, 581, doi: 10.1111/j.1365-2966.2007.12560.x

Endsley, R., Chisholm, J., Stark, D. P., Topping, M. W., & Whitler, L. 2025, ApJ, 987, 189, doi: 10.3847/1538-4357/addc74

Endsley, R., & Stark, D. P. 2022, MNRAS, 511, 6042, doi: 10.1093/mnras/stac524

Endsley, R., Stark, D. P., Bouwens, R. J., et al. 2022, MNRAS, 517, 5642, doi: 10.1093/mnras/stac3064

Endsley, R., Stark, D. P., Whitler, L., et al. 2024, MNRAS, 533, 1111, doi: 10.1093/mnras/stae1857

Federrath, C., Roman-Duval, J., Klessen, R. S., Schmidt, W., & Mac Low, M.-M. 2010, A&A, 512, A81, doi: 10.1051/0004-6361/200912437

Feltre, A., Charlot, S., & Gutkin, J. 2016, MNRAS, 456, 3354, doi: 10.1093/mnras/stv2794

Ferruit, P., Jakobsen, P., Giardino, G., et al. 2022, A&A, 661, A81, doi: 10.1051/0004-6361/202142673

Finley, H., Bouché, N., Contini, T., et al. 2017, A&A, 608, A7, doi: 10.1051/0004-6361/201731499

Francis, P. J., Hewett, P. C., Foltz, C. B., et al. 1991, ApJ, 373, 465, doi: 10.1086/170066

Fujimoto, S., Wang, B., Weaver, J. R., et al. 2024, ApJ, 977, 250, doi: 10.3847/1538-4357/ad9027

Furtak, L. J., Zitrin, A., Plat, A., et al. 2023a, ApJ, 952, 142, doi: 10.3847/1538-4357/acdc9d

Furtak, L. J., Zitrin, A., Weaver, J. R., et al. 2023b, MNRAS, 523, 4568, doi: 10.1093/mnras/stad1627

Furtak, L. J., Labbé, I., Zitrin, A., et al. 2024, Nature, 628, 57, doi: 10.1038/s41586-024-07184-8

Furtak, L. J., Secunda, A. R., Greene, J. E., et al. 2025, A&A, 698, A227, doi: 10.1051/0004-6361/202554110

Gardner, J. P., Mather, J. C., Abbott, R., et al. 2023, PASP, 135, 068001, doi: 10.1088/1538-3873/acd1b5

Glazer, K. S., Jones, T., Chen, Y., et al. 2025, ApJ, 992, 191, doi: 10.3847/1538-4357/ae0194

Gloudemans, A. J., Duncan, K. J., Eilers, A.-C., et al. 2025, ApJ, 986, 130, doi: 10.3847/1538-4357/adddb9

Gordon, K. D., Clayton, G. C., Misselt, K. A., Landolt, A. U., & Wolff, M. J. 2003, ApJ, 594, 279, doi: 10.1086/376774

Grandi, S. A. 1980, ApJ, 238, 10, doi: 10.1086/157952

Greene, J. E., & Ho, L. C. 2005, ApJ, 630, 122, doi: 10.1086/431897

Greene, J. E., Labbe, I., Goulding, A. D., et al. 2024, ApJ, 964, 39, doi: 10.3847/1538-4357/ad1e5f

Gronke, M. 2017, A&A, 608, A139, doi: 10.1051/0004-6361/201731791

Gronke, M., & Dijkstra, M. 2014, MNRAS, 444, 1095, doi: 10.1093/mnras/stu1513

Gronke, M., Dijkstra, M., McCourt, M., & Oh, S. P. 2016, ApJL, 833, L26, doi: 10.3847/2041-8213/833/2/L26

Gronke, M., Dijkstra, M., McCourt, M., & Oh, S. P. 2017, A&A, 607, A71, doi: 10.1051/0004-6361/201731013

Gunn, J. E., & Peterson, B. A. 1965, ApJ, 142, 1633, doi: 10.1086/148444

Gurung-López, S., Gronke, M., Saito, S., Bonoli, S., & Orsi, Á. A. 2022, MNRAS, 510, 4525, doi: 10.1093/mnras/stab3554

Gurung-López, S., Orsi, Á. A., & Bonoli, S. 2019, MNRAS, 490, 733, doi: 10.1093/mnras/stz2591

Guseva, N. G., Izotov, Y. I., Fricke, K. J., & Henkel, C. 2013, A&A, 555, A90, doi: 10.1051/0004-6361/201221010

Gutkin, J., Charlot, S., & Bruzual, G. 2016, MNRAS, 462, 1757, doi: 10.1093/mnras/stw1716

Hansen, M., & Oh, S. P. 2006, MNRAS, 367, 979, doi: 10.1111/j.1365-2966.2005.09870.x

Harikane, Y., Zhang, Y., Nakajima, K., et al. 2023, ApJ, 959, 39, doi: 10.3847/1538-4357/ad029e

Harris, C. R., Millman, K. J., van der Walt, S. J., et al. 2020, Nature, 585, 357, doi: 10.1038/s41586-020-2649-2

Hayes, M. 2015, PASA, 32, e027, doi: 10.1017/pasa.2015.25

Heintz, K. E., Brammer, G. B., Watson, D., et al. 2025, A&A, 693, A60, doi: 10.1051/0004-6361/202450243

Henry, A., Berg, D. A., Scarlata, C., Verhamme, A., & Erb, D. 2018, ApJ, 855, 96, doi: 10.3847/1538-4357/aab099

Henry, A., Scarlata, C., Martin, C. L., & Erb, D. 2015, ApJ, 809, 19, doi: 10.1088/0004-637X/809/1/19

Hu, E. M., Cowie, L. L., & McMahon, R. G. 1998, ApJL, 502, L99, doi: 10.1086/311506

Humphreys, R. M., & Davidson, K. 1994, PASP, 106, 1025, doi: 10.1086/133478

Hunter, J. D. 2007, Computing in Science and Engineering, 9, 90, doi: 10.1109/MCSE.2007.55

Hviding, R. E., de Graaff, A., Miller, T. B., et al. 2025, A&A, 702, A57, doi: 10.1051/0004-6361/202555816

Inayoshi, K., & Maiolino, R. 2025, ApJL, 980, L27, doi: 10.3847/2041-8213/adaebd

Inayoshi, K., Murase, K., & Kashiyama, K. 2026, ApJ, 1000, 90, doi: 10.3847/1538-4357/ae42ce

Isobe, Y., Maiolino, R., D'Eugenio, F., et al. 2025, MNRAS, 541, L71, doi: 10.1093/mnrasl/slaf056

Izotov, Y. I., Schaerer, D., Thuan, T. X., et al. 2016, MNRAS, 461, 3683, doi: 10.1093/mnras/stw1205

Izotov, Y. I., Schaerer, D., Worseck, G., et al. 2018, MNRAS, 474, 4514, doi: 10.1093/mnras/stx3115

Izotov, Y. I., Thuan, T. X., & Privon, G. 2012, MNRAS, 427, 1229, doi: 10.1111/j.1365-2966.2012.22051.x

Jakobsen, P., Ferruit, P., Alves de Oliveira, C., et al. 2022, A&A, 661, A80, doi: 10.1051/0004-6361/202142663

Ji, X., Maiolino, R., Übler, H., et al. 2025, MNRAS, doi: 10.1093/mnras/staf1867

Jones, G. C., Bunker, A. J., Saxena, A., et al. 2025, MNRAS, 536, 2355, doi: 10.1093/mnras/stae2670

Jones, G. C., Übler, H., Maiolino, R., et al. 2026, MNRAS, 546, stag115, doi: 10.1093/mnras/stag115

Jones, T., Stark, D. P., & Ellis, R. S. 2012, ApJ, 751, 51, doi: 10.1088/0004-637X/751/1/51

Juodžbalis, I., Ji, X., Maiolino, R., et al. 2024, MNRAS, 535, 853, doi: 10.1093/mnras/stae2367

Juodžbalis, I., Marconcini, C., D'Eugenio, F., et al. 2025, arXiv e-prints, arXiv:2508.21748, doi: 10.48550/arXiv.2508.21748

Kageura, Y., Ouchi, M., Nakane, M., et al. 2025, ApJS, 278, 33, doi: 10.3847/1538-4365/adc690

Karman, W., Caputi, K. I., Caminha, G. B., et al. 2017, A&A, 599, A28, doi: 10.1051/0004-6361/201629055
Kido, D., Ioka, K., Hotokezaka, K., Inayoshi, K., & Irwin, C. M. 2025, MNRAS, 544, 3407, doi: 10.1093/mnras/staf1898
Kocevski, D. D., Finkelstein, S. L., Barro, G., et al. 2025, ApJ, 986, 126, doi: 10.3847/1538-4357/adbc7d
Kokorev, V., Fujimoto, S., Labbe, I., et al. 2023, ApJL, 957, L7, doi: 10.3847/2041-8213/ad037a
Kokorev, V., Caputi, K. I., Greene, J. E., et al. 2024, ApJ, 968, 38, doi: 10.3847/1538-4357/ad4265
Kokorev, V., Chisholm, J., Naidu, R. P., et al. 2025, arXiv e-prints, arXiv:2511.07515. https://arxiv.org/abs/2511.07515
Kokubo, M., & Harikane, Y. 2025, ApJ, 995, 24, doi: 10.3847/1538-4357/ae119e
Korista, K., Ferland, G., & Baldwin, J. 1997, ApJ, 487, 555, doi: 10.1086/304659
Kwan, J., & Krolik, J. H. 1981, ApJ, 250, 478, doi: 10.1086/159395
Labbe, I., Greene, J. E., Matthee, J., et al. 2024, arXiv e-prints, arXiv:2412.04557, doi: 10.48550/arXiv.2412.04557
Labbe, I., Greene, J. E., Bezanson, R., et al. 2025, ApJ, 978, 92, doi: 10.3847/1538-4357/ad3551
Lambrides, E., Garofali, K., Larson, R., et al. 2024, arXiv e-prints, arXiv:2409.13047, doi: 10.48550/arXiv.2409.13047
Lambrides, E., Larson, R., Hutchison, T., et al. 2025, arXiv e-prints, arXiv:2509.09607, doi: 10.48550/arXiv.2509.09607
Laseter, I. H., Maseda, M. V., Curti, M., et al. 2024, A&A, 681, A70, doi: 10.1051/0004-6361/202347133
Laursen, P., Duval, F., & Östlin, G. 2013, ApJ, 766, 124, doi: 10.1088/0004-637X/766/2/124
Laursen, P., Sommer-Larsen, J., & Andersen, A. C. 2009, ApJ, 704, 1640, doi: 10.1088/0004-637X/704/2/1640
Lin, X., Wang, F., Fan, X., et al. 2024, ApJ, 974, 147, doi: 10.3847/1538-4357/ad6565
Lin, X., Fan, X., Cai, Z., et al. 2026, ApJ, 997, 364, doi: 10.3847/1538-4357/ae2bdf
Liu, H., Jiang, Y.-F., Quataert, E., Greene, J. E., & Ma, Y. 2025, ApJ, 994, 113, doi: 10.3847/1538-4357/ae0c19
Lu, T.-Y., Mason, C. A., Hutter, A., et al. 2024, MNRAS, 528, 4872, doi: 10.1093/mnras/stae266
Luridiana, V., Morisset, C., & Shaw, R. A. 2015, A&A, 573, A42, doi: 10.1051/0004-6361/201323152
Mac Low, M.-M. 1999, ApJ, 524, 169, doi: 10.1086/307784
Madau, P., & Haardt, F. 2024, ApJL, 976, L24, doi: 10.3847/2041-8213/ad90e1
Madau, P., & Maiolino, R. 2026, arXiv e-prints, arXiv:2602.22386, doi: 10.48550/arXiv.2602.22386
Maiolino, R., Scholtz, J., Curtis-Lake, E., et al. 2024a, A&A, 691, A145, doi: 10.1051/0004-6361/202347640
Maiolino, R., Scholtz, J., Witstok, J., et al. 2024b, Nature, 627, 59, doi: 10.1038/s41586-024-07052-5
Maiolino, R., Risaliti, G., Signorini, M., et al. 2025a, MNRAS, 538, 1921, doi: 10.1093/mnras/staf359
Maiolino, R., Uebler, H., D'Eugenio, F., et al. 2025b, arXiv e-prints, arXiv:2505.22567, doi: 10.48550/arXiv.2505.22567
Mason, C. A., Chen, Z., Stark, D. P., et al. 2026, A&A, 705, A114, doi: 10.1051/0004-6361/202553820
Mason, C. A., & Gronke, M. 2020, MNRAS, 499, 1395, doi: 10.1093/mnras/staa2910
Mason, C. A., Treu, T., Dijkstra, M., et al. 2018, ApJ, 856, 2, doi: 10.3847/1538-4357/aab0a7
Matthee, J., Naidu, R. P., Brammer, G., et al. 2024, ApJ, 963, 129, doi: 10.3847/1538-4357/ad2345
Matthee, J., Naidu, R. P., Kotiwale, G., et al. 2025, ApJ, 988, 246, doi: 10.3847/1538-4357/ade886
Matthee, J., Torralba, A., Pezzulli, G., et al. 2026, arXiv e-prints, arXiv:2603.17667, doi: 10.48550/arXiv.2603.17667
Mignoli, M., Feltre, A., Bongiorno, A., et al. 2019, A&A, 626, A9, doi: 10.1051/0004-6361/201935062
Miralda-Escudé, J. 1998, ApJ, 501, 15, doi: 10.1086/305799
Morishita, T., Stiavelli, M., Mason, C. A., et al. 2026, ApJ, 998, 175, doi: 10.3847/1538-4357/ae3a7c
Naidu, R. P., Matthee, J., Kramarenko, I., et al. 2024, arXiv e-prints, arXiv:2410.01874, doi: 10.48550/arXiv.2410.01874
Naidu, R. P., Matthee, J., Katz, H., et al. 2025, arXiv e-prints, arXiv:2503.16596, doi: 10.48550/arXiv.2503.16596
Nakane, M., Ouchi, M., Nakajima, K., et al. 2024, ApJ, 967, 28, doi: 10.3847/1538-4357/ad38c2
Nandal, D., & Loeb, A. 2026, ApJ, 998, 124, doi: 10.3847/1538-4357/ae32f3
Napolitano, L., Pentericci, L., Santini, P., et al. 2024, A&A, 688, A106, doi: 10.1051/0004-6361/202449644
Neufeld, D. A. 1990, ApJ, 350, 216, doi: 10.1086/168375
Neufeld, D. A. 1991, ApJL, 370, L85, doi: 10.1086/185983
Neyer, M., Smith, A., Kannan, R., et al. 2024, MNRAS, 531, 2943, doi: 10.1093/mnras/stae1325
Nikolić, I., Mesinger, A., Mason, C. A., et al. 2025, A&A, 699, A323, doi: 10.1051/0004-6361/202553756
Nikopoulos, G. P., Watson, D., Sneppen, A., et al. 2025, arXiv e-prints, arXiv:2510.06362, doi: 10.48550/arXiv.2510.06362

Ning, Y., Cai, Z., Lin, X., et al. 2024, ApJL, 963, L38, doi: 10.3847/2041-8213/ad292f

Oke, J. B., & Gunn, J. E. 1983, ApJ, 266, 713, doi: 10.1086/160817

Osterbrock, D. E., & Ferland, G. J. 2006, Astrophysics of gaseous nebulae and active galactic nuclei

Pahl, A. J., Shapley, A., Faisst, A. L., et al. 2020, MNRAS, 493, 3194, doi: 10.1093/mnras/staa355

Pentericci, L., Vanzella, E., Castellano, M., et al. 2018, A&A, 619, A147, doi: 10.1051/0004-6361/201732465

Pérez-González, P. G., Barro, G., Rieke, G. H., et al. 2024, ApJ, 968, 4, doi: 10.3847/1538-4357/ad38bb

Plat, A., Charlot, S., Bruzual, G., et al. 2019, MNRAS, 490, 978, doi: 10.1093/mnras/stz2616

Price, S. H., Bezanson, R., Labbe, I., et al. 2025, ApJ, 982, 51, doi: 10.3847/1538-4357/adaec1

Prieto-Lyon, G., Mason, C., Mascia, S., et al. 2023, ApJ, 956, 136, doi: 10.3847/1538-4357/acf715

Qin, Y., Mesinger, A., Prelogović, D., et al. 2025, PASA, 42, e049, doi: 10.1017/pasa.2025.35

Quider, A. M., Pettini, M., Shapley, A. E., & Steidel, C. C. 2009, MNRAS, 398, 1263, doi: 10.1111/j.1365-2966.2009.15234.x

Rafiee, A., Pirkola, P., Hall, P. B., et al. 2016, MNRAS, 459, 2472, doi: 10.1093/mnras/stw634

Reddy, N. A., Steidel, C. C., Pettini, M., Bogosavljević, M., & Shapley, A. E. 2016, ApJ, 828, 108, doi: 10.3847/0004-637X/828/2/108

Reines, A. E., & Volonteri, M. 2015, ApJ, 813, 82, doi: 10.1088/0004-637X/813/2/82

Rieke, M. J., Kelly, D. M., Misselt, K., et al. 2023, PASP, 135, 028001, doi: 10.1088/1538-3873/acac53

Rigby, J., Perrin, M., McElwain, M., et al. 2023, PASP, 135, 048001, doi: 10.1088/1538-3873/acb293

Rix, S. A., Pettini, M., Leitherer, C., et al. 2004, ApJ, 615, 98, doi: 10.1086/424031

Roberts-Borsani, G., Treu, T., Shapley, A., et al. 2024, ApJ, 976, 193, doi: 10.3847/1538-4357/ad85d3

Rodríguez-Ardila, A., Viegas, S. M., Pastoriza, M. G., Prato, L., & Donzelli, C. J. 2002, ApJ, 572, 94, doi: 10.1086/340192

Rodríguez Hidalgo, P., Hamann, F., & Hall, P. 2011, MNRAS, 411, 247, doi: 10.1111/j.1365-2966.2010.17677.x

Rose, M., Tadhunter, C. N., Holt, J., Ramos Almeida, C., & Littlefair, S. P. 2011, MNRAS, 414, 3360, doi: 10.1111/j.1365-2966.2011.18639.x

Rubin, K. H. R., Weiner, B. J., Koo, D. C., et al. 2010, ApJ, 719, 1503, doi: 10.1088/0004-637X/719/2/1503

Rusakov, V., Watson, D., Nikopoulos, G. P., et al. 2026, Nature, 649, 574, doi: 10.1038/s41586-025-09900-4

Sanders, R. L., Shapley, A. E., Topping, M. W., Reddy, N. A., & Brammer, G. B. 2023, ApJ, 955, 54, doi: 10.3847/1538-4357/acedad

Sanders, R. L., Shapley, A. E., Topping, M. W., Reddy, N. A., & Brammer, G. B. 2024, ApJ, 962, 24, doi: 10.3847/1538-4357/ad15fc

Sanders, R. L., Shapley, A. E., Reddy, N. A., et al. 2020, MNRAS, 491, 1427, doi: 10.1093/mnras/stz3032

Saxena, A., Robertson, B. E., Bunker, A. J., et al. 2023, A&A, 678, A68, doi: 10.1051/0004-6361/202346245

Saxena, A., Bunker, A. J., Jones, G. C., et al. 2024, A&A, 684, A84, doi: 10.1051/0004-6361/202347132

Schenker, M. A., Ellis, R. S., Konidaris, N. P., & Stark, D. P. 2014, ApJ, 795, 20, doi: 10.1088/0004-637X/795/1/20

Schindler, J.-T., Hennawi, J. F., Davies, F. B., et al. 2025, Nature Astronomy, 9, 1732, doi: 10.1038/s41550-025-02660-1

Scholtz, J., D'Eugenio, F., Maiolino, R., et al. 2026, arXiv e-prints, arXiv:2603.22277, doi: 10.48550/arXiv.2603.22277

Senchyna, P., Stark, D. P., Chevallard, J., et al. 2019, MNRAS, 488, 3492, doi: 10.1093/mnras/stz1907

Setton, D. J., Greene, J. E., Spilker, J. S., et al. 2025, ApJL, 991, L10, doi: 10.3847/2041-8213/ade78b

Shapley, A. E., Reddy, N. A., Sanders, R. L., Topping, M. W., & Brammer, G. B. 2023, ApJL, 950, L1, doi: 10.3847/2041-8213/acd939

Shapley, A. E., Steidel, C. C., Pettini, M., & Adelberger, K. L. 2003, ApJ, 588, 65, doi: 10.1086/373922

Sigut, T. A. A., & Pradhan, A. K. 2003, ApJS, 145, 15, doi: 10.1086/345498

Sneppen, A., Watson, D., Matthews, J. H., et al. 2026, arXiv e-prints, arXiv:2601.18864, doi: 10.48550/arXiv.2601.18864

Stark, D. P., Ellis, R. S., & Ouchi, M. 2011, ApJL, 728, L2, doi: 10.1088/2041-8205/728/1/L2

Steidel, C. C., Strom, A. L., Pettini, M., et al. 2016, ApJ, 826, 159, doi: 10.3847/0004-637X/826/2/159

Sun, W. Q., Naidu, R. P., Matthee, J., et al. 2026, arXiv e-prints, arXiv:2601.20929, doi: 10.48550/arXiv.2601.20929

Tang, M., Stark, D. P., Chevallard, J., & Charlot, S. 2019, MNRAS, 489, 2572, doi: 10.1093/mnras/stz2236

Tang, M., Stark, D. P., Ellis, R. S., et al. 2024a, ApJ, 972, 56, doi: 10.3847/1538-4357/ad5ae0

Tang, M., Stark, D. P., Mason, C. A., et al. 2025a, arXiv e-prints, arXiv:2507.08245, doi: 10.48550/arXiv.2507.08245

Tang, M., Stark, D. P., Topping, M. W., Mason, C., & Ellis, R. S. 2024b, ApJ, 975, 208, doi: 10.3847/1538-4357/ad7eb7

Tang, M., Stark, D. P., Ellis, R. S., et al. 2024c, MNRAS, 531, 2701, doi: 10.1093/mnras/stae1338

Tang, M., Stark, D. P., Plat, A., et al. 2025b, ApJ, 991, 217, doi: 10.3847/1538-4357/adfd57

Taylor, A. J., Kokorev, V., Kocevski, D. D., et al. 2025, ApJL, 989, L7, doi: 10.3847/2041-8213/ade789

Tee, W. L., Fan, X., Wang, F., & Yang, J. 2025, ApJL, 983, L26, doi: 10.3847/2041-8213/adc5e3

Terao, K., Nagao, T., Onishi, K., et al. 2022, ApJ, 929, 51, doi: 10.3847/1538-4357/ac5b71

Topping, M. W., Stark, D. P., Senchyna, P., et al. 2025, ApJ, 980, 225, doi: 10.3847/1538-4357/ada95c

Torralba, A., Matthee, J., Pezzulli, G., et al. 2026a, A&A, 707, A75, doi: 10.1051/0004-6361/202557537

Torralba, A., Matthee, J., Pezzulli, G., et al. 2026b, A&A, 705, A147, doi: 10.1051/0004-6361/202555596

Treiber, H., Greene, J. E., Weaver, J. R., et al. 2025, ApJ, 984, 93, doi: 10.3847/1538-4357/adc38f

Tripodi, R., Bradač, M., D'Eugenio, F., et al. 2025, ApJL, 994, L6, doi: 10.3847/2041-8213/ae13a9

Umeda, H., Inayoshi, K., Harikane, Y., & Murase, K. 2026a, ApJ, 999, 183, doi: 10.3847/1538-4357/ae4101

Umeda, H., Ouchi, M., Kageura, Y., et al. 2026b, ApJ, 997, 86, doi: 10.3847/1538-4357/ae232b

Vanden Berk, D. E., Richards, G. T., Bauer, A., et al. 2001, AJ, 122, 549, doi: 10.1086/321167

Vázquez-Semadeni, E., Cantó, J., & Lizano, S. 1998, ApJ, 492, 596, doi: 10.1086/305064

Verhamme, A., Schaerer, D., & Maselli, A. 2006, A&A, 460, 397, doi: 10.1051/0004-6361:20065554

Vidal-García, A., Charlot, S., Bruzual, G., & Hubeny, I. 2017, MNRAS, 470, 3532, doi: 10.1093/mnras/stx1324

Virtanen, P., Gommers, R., Oliphant, T. E., et al. 2020, Nature Methods, 17, 261, doi: 10.1038/s41592-019-0686-2

Wang, B., Leja, J., de Graaff, A., et al. 2024, ApJL, 969, L13, doi: 10.3847/2041-8213/ad55f7

Wang, B., Leja, J., Katz, H., et al. 2025a, arXiv e-prints, arXiv:2508.18358, doi: 10.48550/arXiv.2508.18358

Wang, B., de Graaff, A., Davies, R. L., et al. 2025b, ApJ, 984, 121, doi: 10.3847/1538-4357/adc1ca

Whitler, L., Stark, D. P., Mason, C. A., et al. 2025, arXiv e-prints, arXiv:2510.12019, doi: 10.48550/arXiv.2510.12019

Williams, C. C., Alberts, S., Ji, Z., et al. 2024, ApJ, 968, 34, doi: 10.3847/1538-4357/ad3f17

Wills, B. J., Netzer, H., & Wills, D. 1985, ApJ, 288, 94, doi: 10.1086/162767

Witstok, J., Smit, R., Saxena, A., et al. 2024, A&A, 682, A40, doi: 10.1051/0004-6361/202347176

Witstok, J., Maiolino, R., Smit, R., et al. 2025, MNRAS, 536, 27, doi: 10.1093/mnras/stae2535

Xiao, M., Oesch, P. A., Bing, L., et al. 2025, A&A, 700, A231, doi: 10.1051/0004-6361/202554361

Yue, M., Eilers, A.-C., Ananna, T. T., et al. 2024, ApJL, 974, L26, doi: 10.3847/2041-8213/ad7eba

Zakamska, N. L., Strauss, M. A., Krolik, J. H., et al. 2003, AJ, 126, 2125, doi: 10.1086/378610

Zhang, Z., Jiang, L., Liu, W., & Ho, L. C. 2025, ApJ, 985, 119, doi: 10.3847/1538-4357/adcb3e

Zwick, L., Tiede, C., & Mayer, L. 2025, arXiv e-prints, arXiv:2507.22014, doi: 10.48550/arXiv.2507.22014